ARTICLES
https://doi.org/10.1038/s41593-018-0110-8
nature neuroscience

Social deficits in *Shank3*-deficient mouse models of autism are rescued by histone deacetylase (HDAC) inhibition

Luye Qin[1], Kaijie Ma[1], Zi-Jun Wang[1], Zihua Hu[2], Emmanuel Matas[1], Jing Wei[1] and Zhen Yan[1*]

Haploinsufficiency of the *SHANK3* gene is causally linked to autism spectrum disorder (ASD), and ASD-associated genes are also enriched for chromatin remodelers. Here we found that brief treatment with romidepsin, a highly potent class I histone deacetylase (HDAC) inhibitor, alleviated social deficits in *Shank3*-deficient mice, which persisted for ~3 weeks. *HDAC2* transcription was upregulated in these mice, and knockdown of *HDAC2* in prefrontal cortex also rescued their social deficits. Nuclear localization of β-catenin, a Shank3-binding protein that regulates cell adhesion and transcription, was increased in *Shank3*-deficient mice, which induced *HDAC2* upregulation and social deficits. At the downstream molecular level, romidepsin treatment elevated the expression and histone acetylation of *Grin2a* and actin-regulatory genes and restored NMDA-receptor function and actin filaments in *Shank3*-deficient mice. Taken together, these findings highlight an epigenetic mechanism underlying social deficits linked to *Shank3* deficiency, which may suggest potential therapeutic strategies for ASD patients bearing *SHANK3* mutations.

Mouse models that reflect the core symptoms of ASD, including deficits in sociability and repetitive behaviors, are crucial for preclinical investigations of pathophysiological mechanisms and novel treatment avenues[1]. Haploinsufficiency of the *SHANK3* gene, which encodes a master scaffolding protein in the postsynaptic density of glutamatergic synapses[2], is causally linked to 22q13.3 deletion syndrome (also known as Phelan–McDermid syndrome), which conveys a high risk for ASD[3–6]. Deletion or loss-of-function mutations of one copy of *SHANK3* account for 0.5–2.0% of ASD and intellectual disability cases[5,6]. Human genetic studies of ASD have found that enriched mutations are located at the *SHANK3* C-terminal region (exon 21)[4], which contains binding sites for actin (and cortactin) and mGluR (and Homer) and plays a crucial role in the synaptic targeting and postsynaptic assembly of Shank3 complex.

Mouse models with *Shank3* deficiency exhibit autism-associated behaviors to different extents[7–16]. Male heterozygous mice with C-terminal (exon 21) deleted *Shank3* (Shank3$^{+/\Delta C}$), which exhibit reduced full-length Shank3 expression[11,12] and loss of synaptic localization of the truncated Shank3 protein[12], recapitulate social preference deficits and repetitive behaviors[12]. These behavioral deficits in *Shank3*$^{+/\Delta C}$ mice are attributable to the loss of NMDA-receptor (NMDAR) function and synaptic trafficking due to actin dysregulation in pyramidal neurons of prefrontal cortex (PFC)[12], a brain region that plays an essential role in mediating social cognition[17].

Large-scale genetic studies have revealed that many ASD-associated genes are involved in synaptic homeostasis, transcriptional regulation and chromatin-remodeling pathways[18–21]. This prompted us to speculate that targeting epigenetic enzymes to normalize gene expression and ameliorate synaptic defects may be a potential strategy to relieve social deficits in ASD. Here we targeted HDAC family proteins, which generally cause silencing of gene expression via condensing the chromatin architecture. HDACs play a key role in cognitive processes[22,23], and altered histone acetylation and transcriptional dysfunction have been implicated in psychiatric disorders[24]; however, the efficacy of HDAC-targeting agents in models of ASD is unknown. Here we have identified an HDAC inhibitor that persistently alleviates social deficits in *Shank3*-deficient mice.

Results

Treatment with the HDAC inhibitor romidepsin lastingly relieves autism-like social deficits in *Shank3*-deficient mice. The level of global H3 acetylation (Fig. 1a) in the frontal cortex of Shank3$^{+/\Delta C}$ mice was significantly lower than that from wild-type (WT) mice. A systemic administration of low-dose romidepsin (0.25 mg/kg, intraperitoneally (i.p.), once daily for 3 d), a highly potent and brain-permeable class I-specific HDAC inhibitor (with nanomolar in vitro potency[25]) approved by the US Food and Drug Administration (FDA) for cancer treatment[26–28], significantly elevated the level of acetylated H3 in Shank3$^{+/\Delta C}$ mice, while it had little effect in WT mice. These data suggest that *Shank3*-deficient mice have an abnormally low level of histone acetylation, which can be restored by romidepsin treatment.

Next, we examined the impact of romidepsin on social deficits in young (5–6 weeks old) male Shank3$^{+/\Delta C}$ mice, which exhibit loss of social preference in the three-chamber social-interaction assay[12]. As shown in Fig. 1b,d, during the presentation of both social (Soc) and nonsocial (NS) stimuli, romidepsin (0.25 mg/kg, i.p, 3×)-treated Shank3$^{+/\Delta C}$ mice spent significantly more time exploring the social stimulus over the nonsocial object, similarly to WT mice, while saline-injected Shank3$^{+/\Delta C}$ mice showed a significant loss of the preference for the social stimulus. WT mice treated with romidepsin had unchanged social preferences. The significantly elevated social preference index in Shank3$^{+/\Delta C}$ mice after romidepsin treatment (Fig. 1c) suggests that romidepsin alleviates the observed social deficits.

[1]Department of Physiology and Biophysics, Jacobs School of Medicine and Biomedical Sciences, State University of New York at Buffalo, Buffalo, NY, USA. [2]Center for Computational Research, New York State Center of Excellence in Bioinformatics & Life Sciences, State University of New York at Buffalo, Buffalo, NY, USA. These authors contributed equally: Luye Qin and Kaijie Ma. *e-mail: zhenyan@buffalo.edu

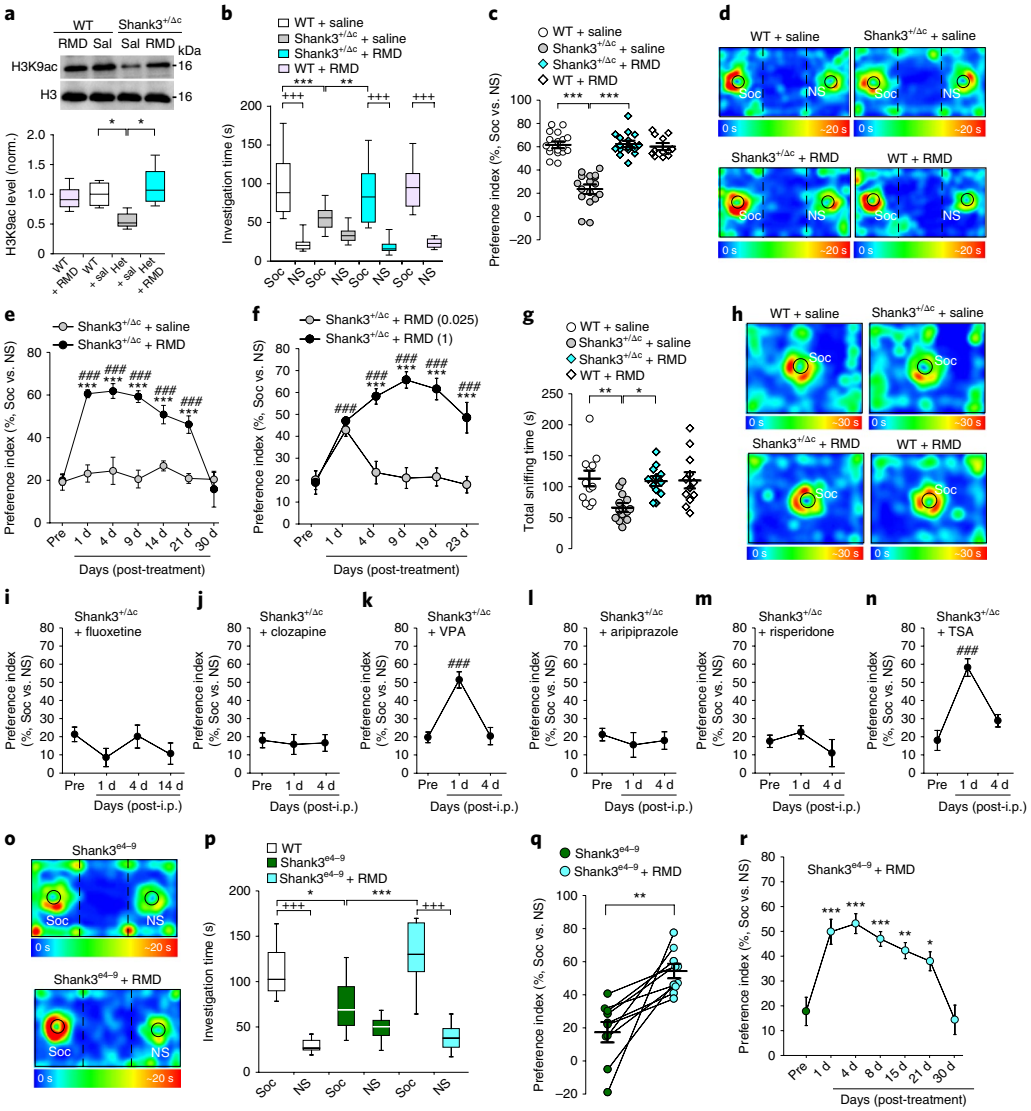

Fig. 1 | Treatment with the HDAC inhibitor romidepsin induces robust, prolonged rescue of autism-like social deficits in *Shank3*-deficient mice, while a variety of drugs for psychiatric disorders fail to do so. a, Immunoblots and quantification analysis of the level of acetylated H3 and total H3 in the nuclear fraction of cortical slices from WT or Shank3$^{+/\Delta C}$ (Het) mice injected (i.p.) with saline (sal) or romidepsin (RMD, 0.25 mg/kg, 3×). Immunoblotting was performed 4–5 d postinjection ($F_{1,20}=11.3$, $P=0.0031$; $^{*}P<0.05$, two-way ANOVA, $n=6$ mice per group). **b**,**c**, Plots showing the time spent investigating either the social (Soc) or nonsocial (NS) stimulus (**b**) and the social preference index (**c**) during three-chamber sociability testing of saline-injected WT ($n=18$), saline-injected Shank3$^{+/\Delta C}$ ($n=17$), RMD-treated Shank3$^{+/\Delta C}$ ($n=17$) and RMD-treated WT ($n=12$) mice (**b**: $F_{3,120}=11.4$, $P<0.0001$; $^{+++}P<0.001$, Soc vs. NS, $^{**}P<0.01$, $^{***}P<0.001$, two-way ANOVA; **c**: $F_{1,60}=58.5$, $P<0.0001$; $^{***}P<0.001$, two-way ANOVA). **d**, Representative heat maps illustrating the time spent by all groups in different locations of the three chambers from the social preference tests. Soc and NS stimuli are labeled with the circles. **e**, Plots of social preference index in Shank3$^{+/\Delta C}$ mice treated with RMD ($n=10$) or saline ($n=10$) at different timepoints ($F_{1,18(\text{treatment})}=124.3$, $P<0.0001$; $^{***}P<0.001$, saline vs. RMD; $^{\#\#\#}P<0.001$, preinjection vs. postinjection, two-way repeated-measures ANOVA). **f**, Plots of social preference index in Shank3$^{+/\Delta C}$ mice treated with different doses of RMD (0.025 mg/kg, $n=9$; 1 mg/kg, $n=8$) at different timepoints ($F_{1,15(\text{treatment})}=51.3$, $P<0.0001$; $^{***}P<0.001$, 1 mg/kg vs. 0.025 mg/kg RMD; $^{\#\#\#}P<0.001$, preinjection vs. postinjection, two-way repeated-measures ANOVA). **g**, Scatter plots showing total sniffing time in social-approach tests of saline-injected WT ($n=12$), saline-injected Shank3$^{+/\Delta C}$ ($n=14$), RMD-treated Shank3$^{+/\Delta C}$ ($n=12$) and RMD-treated WT ($n=12$) mice ($F_{1,46}=6.0$, $P=0.018$; $^{*}P<0.05$, $^{**}P<0.01$, two-way ANOVA). **h**, Representative heat maps illustrating time spent in different locations of the apparatus from social approach tests of all groups. Locations of social stimuli are labeled with circles. **i**–**n**, Plots of social preference index in Shank3$^{+/\Delta C}$ mice treated with (**i**) fluoxetine (10 mg/kg, i.p., 14×, $n=9$), (**j**) clozapine (5 mg/kg, i.p., 3×, $n=11$), (**k**) valproic acid (VPA, 100 mg/kg, i.p., 3×, $n=11$), (**l**) aripiprazole (1 mg/kg, i.p., 3×, $n=9$), (**m**) risperidone (0.1 mg/kg, i.p., 3×, $n=10$) or (**n**) trichostatin A (TSA, 0.5 mg/kg, i.p., 3×, $n=8$; $F_{2,30}=19.2$ (VPA), $P<0.0001$; $F_{2,21}=19.7$, $P<0.0001$ (TSA); $^{\#\#\#}P<0.001$ (preinjection vs. postinjection), one-way ANOVA.) **o**, Representative heat maps illustrating the time spent in different locations of the three chambers from the social preference tests of a Shank3^{e4-9} mouse before and after RMD treatment (0.25 mg/kg, i.p., 3×). **p**, Box plots showing the time spent investigating either Soc or NS stimulus during sociability testing in WT ($n=8$) or homozygous Shank3^{e4-9} mice ($n=10$) before and after RMD treatment ($F_{2,50}=9.2$, $P=0.0003$; $^{+++}P<0.001$, Soc vs. NS; $^{*}P<0.05$, $^{***}P<0.001$, two-way ANOVA). **q**, Scatter plots showing the preference index of the sociability testing in individual Shank3^{e4-9} mice before and after RMD treatment ($n=10$; $t_9=4.36$, $^{**}P=0.0018$, paired two-tailed t test). **r**, Plots of social preference index in Shank3^{e4-9} mice ($n=10$) treated with RMD at different timepoints ($F_{6,63}=11.8$, $P<0.0001$; $^{*}P<0.05$, $^{**}P<0.01$, $^{***}P<0.001$, preinjection vs. postinjection, one-way ANOVA). Shank3$^{+/\Delta C}$ mice (**a**–**n**) and WT mice (**a**–**n**,**p**) are all males, 5–6 weeks old; Shank3^{e4-9} mice (**o**–**r**) are 6 males and 4 females, 5–6 weeks old. Data are presented as median with interquartile ranges (**a**,**b**,**p**) or mean ± s.e.m. (**c**,**e**–**g**,**i**–**n**,**q**,**r**). Each set of the experiments was replicated at least three times. See Supplementary Fig. 8 for blot source data.

We then examined how long the effect of a brief romidepsin treatment could last. Social preference assays were performed in Shank3$^{+/\Delta C}$ mice before and at various timepoints after drug treatment. As shown in Fig. 1e, the significantly increased social preference index in Shank3$^{+/\Delta C}$ mice persisted for at least 21 d postinjection of romidepsin, while no improvement in social preference was found with repeated measurements of saline-injected Shank3$^{+/\Delta C}$ mice. Romidepsin treatment not only persistently improved social preference, but also induced a sustained increase in the time spent interacting with the social stimulus in young Shank3$^{+/\Delta C}$ mice (Supplementary Fig. 1a,b). The prolonged effect of romidepsin is consistent with the long duration of human response to romidepsin (13.7 months) revealed by pharmacokinetics analyses[26,27]. Romidepsin treatment of adult Shank3$^{+/\Delta C}$ mice gave a less potent and more transient effect on social behaviors (Supplementary Fig. 1c,d), suggesting that the therapeutic efficacy of the drug is influenced by developmental processes.

The effective dose of romidepsin in rescuing social deficits (0.25 mg/kg, i.e., 0.75 mg/m^2, i.p., once daily for 3 d) is equivalent to ~5% of the clinical anticancer dose in humans (14 mg/m^2, intravenously, once a week for 3 weeks). Dose-response studies (Fig. 1f) indicated that a higher dose of romidepsin (1 mg/kg, i.p., 3×) had similar long-lasting rescuing effects on the social preference behavior in Shank3$^{+/\Delta C}$ mice, while a lower dose (0.025 mg/kg, i.p., 3×) was ineffective in improving the social deficits persistently. Thus, 0.25 mg/kg romidepsin was used in the following studies.

We further examined the impact of romidepsin on social approach behaviors in young Shank3$^{+/\Delta C}$ mice. As shown in Fig. 1g,h, compared to WT mice, Shank3$^{+/\Delta C}$ mice spent significantly less time approaching and interacting with social stimuli, which was almost completely reversed by romidepsin treatment. Taken together, these results suggest that brief treatment with low-dose romidepsin can lead to prolonged rescue of autism-like social deficits in the *Shank3*-deficient model.

Moreover, we examined whether other pharmacological agents currently used for various psychiatric disorders were able to rescue autism-like social deficits in Shank3$^{+/\Delta C}$ mice. As shown in Fig. 1i, treatment with the selective serotonin reuptake inhibitor (SSRI) antidepressant fluoxetine (once daily for 14 d) failed to induce any improvement in social preference in the three-chamber social-interaction assay. The atypical antipsychotics clozapine (once daily for 3 d) was also ineffective in rescuing social deficits (Fig. 1j). The mood stabilizer valproic acid (once daily for 3 d), a low-affinity class I HDAC inhibitor (with millimolar in vitro potency[25]), only transiently increased the social preference index, but this effect disappeared within a few days after the end of treatment (Fig. 1k). No improvement in social preference was observed with aripiprazole (once daily for 3 d; Fig. 1l) or risperidone (once daily for 3 d; Fig. 1m), the only drugs approved by FDA for ASD treatment, which is consistent with the lack of effect of these drugs on the social communication deficits observed in ASD patients despite their utility in managing irritability and repetitive behaviors[29]. All these antipsychotics failed to increase the time spent interacting with the social stimulus in Shank3$^{+/\Delta C}$ mice (Supplementary Fig. 2a–e). Treatment with the pan-HDAC inhibitor trichostatin A (once daily for 3 d) significantly but transiently increased social preference index (Fig. 1n) and social interaction time (Supplementary Fig. 2f,g) in Shank3$^{+/\Delta C}$ mice. These data suggest that the potent and prolonged effectiveness of romidepsin in alleviating social deficits is unique.

To examine the generalizability of the rescue effect of romidepsin on social deficits, we examined another *Shank3*-deficient model, Shank3^{e4-9} mice, which exhibit the loss of major Shank3 isoforms because of the deletion of N-terminal exons 4–9 (ref. [10]). As shown in Fig. 1o–q, in the three-chamber sociability test, homozygous Shank3^{e4-9} mice had significantly impaired social preference, consistent with previous findings[10]. After romidepsin treatment (0.25 mg/kg, i.p, 3×), the social interaction time and social preference index were significantly elevated. Moreover, the rescue effect of romidepsin in Shank3^{e4-9} mice was sustained for ~3 weeks (Fig. 1r), similarly to what was found in Shank3$^{+/\Delta C}$ mice. These results suggest that romidepsin is generally efficacious in mouse models of *Shank3* deficiency.

A variety of other behaviors were also examined in romidepsin-treated young Shank3$^{+/\Delta C}$ mice. Compared to WT mice or saline-injected Shank3$^{+/\Delta C}$ mice, no differences were observed with romidepsin treatment in locomotion tests (Fig. 2a). Rotarod tests also found no difference with romidepsin treatment (Fig. 2b). Romidepsin- or saline-treated Shank3$^{+/\Delta C}$ mice spent similar amounts of time in the center in open-field tests, compared to WT mice (Fig. 2c). These data suggest that romidepsin does not alter motor coordination or anxiety-like behavior. Romidepsin failed to normalize the increased repetitive grooming in Shank3$^{+/\Delta C}$ mice (Fig. 2d).

Romidepsin treatment did not cause nonspecific behavioral effects, suggesting that it is generally safe, consistent with comprehensive safety studies showing that this FDA-approved anticancer drug is safe and well-tolerated[26,28]. To further examine the potential neuronal toxicity of low-dose romidepsin treatment in young Shank3$^{+/\Delta C}$ mice, we performed immunocytochemical experiments to compare neural survival rates. Pyramidal neurons were immunostained with CaMKII and NeuN, and cell density was counted in the PFC region. As shown in Fig. 2e,f, neuronal morphology and density were not altered by romidepsin treatment.

***HDAC2* is upregulated in *Shank3*-deficient mice via a β-catenin-mediated transcriptional mechanism.** To find out which HDAC family member may mediate the therapeutic effect of romidepsin, we first examined the expression of class I HDACs. Quantitative PCR analyses indicated that the level of *HDAC2* mRNA was significantly higher in PFC lysates from Shank3$^{+/\Delta C}$ mice, while the level of *HDAC1*, *HDAC3* and *HDAC8* mRNA was largely unchanged (Fig. 3a). Western blot analyses showed that the protein level of HDAC2, but not HDAC1, in the nucleus fraction of PFC was significantly higher in Shank3$^{+/\Delta C}$ mice (Fig. 3b). Significantly elevated *HDAC2* mRNA and HDAC2 protein were also detected in the PFC of Shank3^{e4-9} mice (Fig. 3c). This suggests that upregulated HDAC2 may be responsible for the abnormally low histone acetylation in *Shank3*-deficient mice.

Next, we tested whether knockdown of *HDAC2* by a stereotaxic injection of HDAC2 short hairpin RNA (shRNA) lentivirus to medial PFC of Shank3$^{+/\Delta C}$ mice might rescue the social deficits. To prevent potential off-target effects, two shRNA lentiviruses targeting different sequences of the mouse *HDAC2* gene (HDAC2 shRNA-1 and HDAC2 shRNA-2) were used. As shown in Fig. 3d, compared to a scrambled control shRNA, HDAC2 shRNA-1 specifically knocked down the mRNA level of *HDAC2*, but not other class I HDAC family members. HDAC2 shRNA-2 was also highly effective in suppressing *HDAC2* mRNA. The level of HDAC2 protein was significantly diminished by injecting these HDAC2 shRNA lentiviruses in vivo. Behavioral assays indicated that Shank3$^{+/\Delta C}$ mice with PFC injection of either HDAC2 shRNA-1 or HDAC2 shRNA-2 lentivirus exhibited significantly increased social interaction times and improved preferences for social stimuli over nonsocial objects in three-chamber sociability tests (Fig. 3e–g). These data suggest that knockdown of *HDAC2* in PFC induces a similar rescuing effect as romidepsin treatment on social deficits.

To understand how the loss of Shank3 at synapses leads to the upregulation of *HDAC2* transcription in the nucleus, we turned our attention to β-catenin, a nucleocytoplasmic shuttle protein involved in both cell adhesion and transcriptional regulation[30]. In the default state, β-catenin is phosphorylated and retained in the cytoplasm, where it is constitutively targeted for proteasomal degradation.

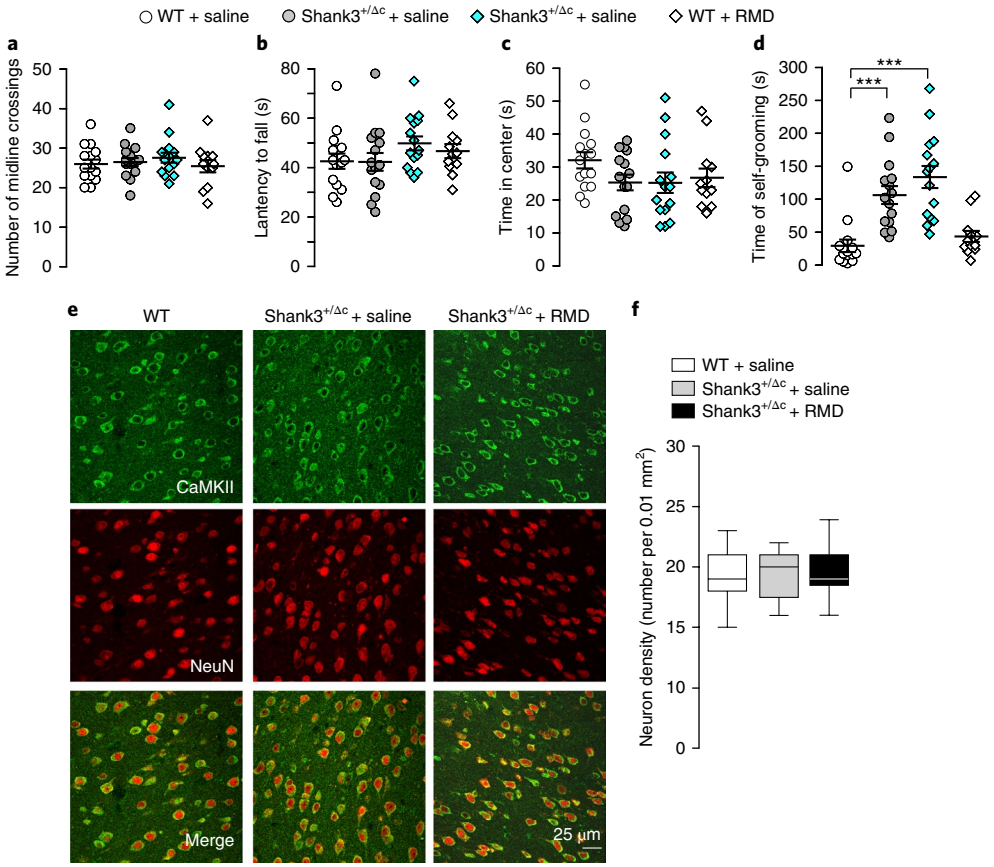

Fig. 2 | Romidepsin treatment does not affect locomotion, anxiety-like behavior or neuronal survival in *Shank3*-deficient mice. a–d, Scatter plots showing a variety of behaviors in saline-injected WT ($n=15$), saline-injected Shank3$^{+/\Delta C}$ ($n=15$), romidepsin (RMD, 0.25 mg/kg, 3×)-treated Shank3$^{+/\Delta C}$ ($n=15$) and RMD-treated WT ($n=12$) mice, including the number of midline crossing in locomotion tests (**a**), the latency to fall during rotarod tests (**b**), the time spent in the center during open-field tests (**c**) and the time spent self-grooming (**d**; $F_{1,53(\text{treatment})}=2.55$, $P=0.117$; $^{***}P<0.001$, two-way ANOVA). **e**,**f**, Confocal images (**e**) and quantification (**f**) of layer V PFC neurons (immunostained with CaMKII and NeuN) in WT or Shank3$^{+/\Delta C}$ mice treated with saline or RMD. Slices were collected for immunostaining 4–5 d postinjection ($n=27$ images from 3 mice per group). All animals used are males, 5–6 weeks old. Data are presented as mean ± s.e.m. (**a–d**) or median with interquartile ranges (**f**). Each set of experiments was replicated at least three times.

Activation of Wnt signaling results in the nuclear translocation of β-catenin, where it activates target genes in a complex with LEF–TCF transcription factors. Neural activity induces the redistribution of β-catenin into spines, where it interacts with the adhesion molecule cadherin to influence synaptic size and strength[31]. β-catenin has also been identified as a critical mediator of dendritic morphogenesis via interacting with cadherin to stabilize actin cytoskeleton[32]. Our co-immunoprecipitation experiments revealed that β-catenin bound to Shank3 in WT mice (Fig. 4a). In PFC of Shank3$^{+/\Delta C}$ mice, β-catenin at the synaptic membrane fraction was significantly reduced, while the level of active (nonphosphorylated) β-catenin in the cytosol and the level of β-catenin in the nucleus were significantly elevated (Fig. 4b). Decreased synaptic β-catenin and increased nuclear β-catenin were also observed in PFC of Shank3^{e4-9} mice (Fig. 4c). These results suggest that *Shank3* deficiency induces the redistribution of β-catenin from synapses to nucleus, probably due to the attenuated association of β-catenin with synaptic scaffolding proteins and adhesion molecules.

The increased nuclear translocation of β-catenin in *Shank3*-deficient mice suggests that it can activate the TCF–LEF transcriptional machinery to regulate target genes. Our chromatin immunoprecipitation (ChIP) assays indicated that β-catenin specifically associated with the *HDAC2* promoter region containing TCF–LEF binding elements (Fig. 4d). β-catenin enrichment on the *HDAC2* promoter was significantly increased in PFC of Shank3$^{+/\Delta C}$ mice (Fig. 4e), implicating β-catenin in the upregulated transcription of *HDAC2*. Other β-catenin target genes found in cancer cells or neural stem cells, such as *Vegf*, *Jun* (encoding c-Jun), *Ccnd1* (encoding Cyclin D1) and *Neurod1*, were not significantly altered in PFC of Shank3$^{+/\Delta C}$ mice (Fig. 4f).

To further reveal the involvement of β-catenin in the regulation of genes and behaviors, we elevated β-catenin expression by injecting β-catenin-expressing adenovirus into the PFC of WT mice. A high level of β-catenin was found in the nucleus of PFC pyramidal neurons (Fig. 4g). *HDAC2* mRNA was significantly and specifically upregulated by β-catenin overexpression in PFC of WT mice (Fig. 4h), similarly to what was found in Shank3$^{+/\Delta C}$ mice. Moreover, social preference deficits were induced in WT mice with elevated β-catenin expression in PFC (Fig. 4i–k), reminiscent of the behavioral consequence of upregulated nuclear β-catenin in *Shank3*-deficient mice.

Next, we diminished β-catenin expression by injecting β-catenin shRNA lentivirus into the PFC of *Shank3*-deficient mice. Effective knockdown of β-catenin expression in vivo was achieved with β-catenin shRNA (Fig. 4l). HDAC2 expression in PFC was significantly reduced in β-catenin shRNA-injected Shank3$^{+/\Delta C}$ mice, compared to those injected with a scrambled control shRNA (Fig. 4m). Furthermore, Shank3$^{+/\Delta C}$ mice with β-catenin knockdown in PFC exhibited significantly increased social interaction times and social preference in three-chamber sociability tests (Fig. 4n–p). Taken together, these results provide direct evidence of the sufficiency and necessity of β-catenin in the regulation of HDAC2 and social behavior.

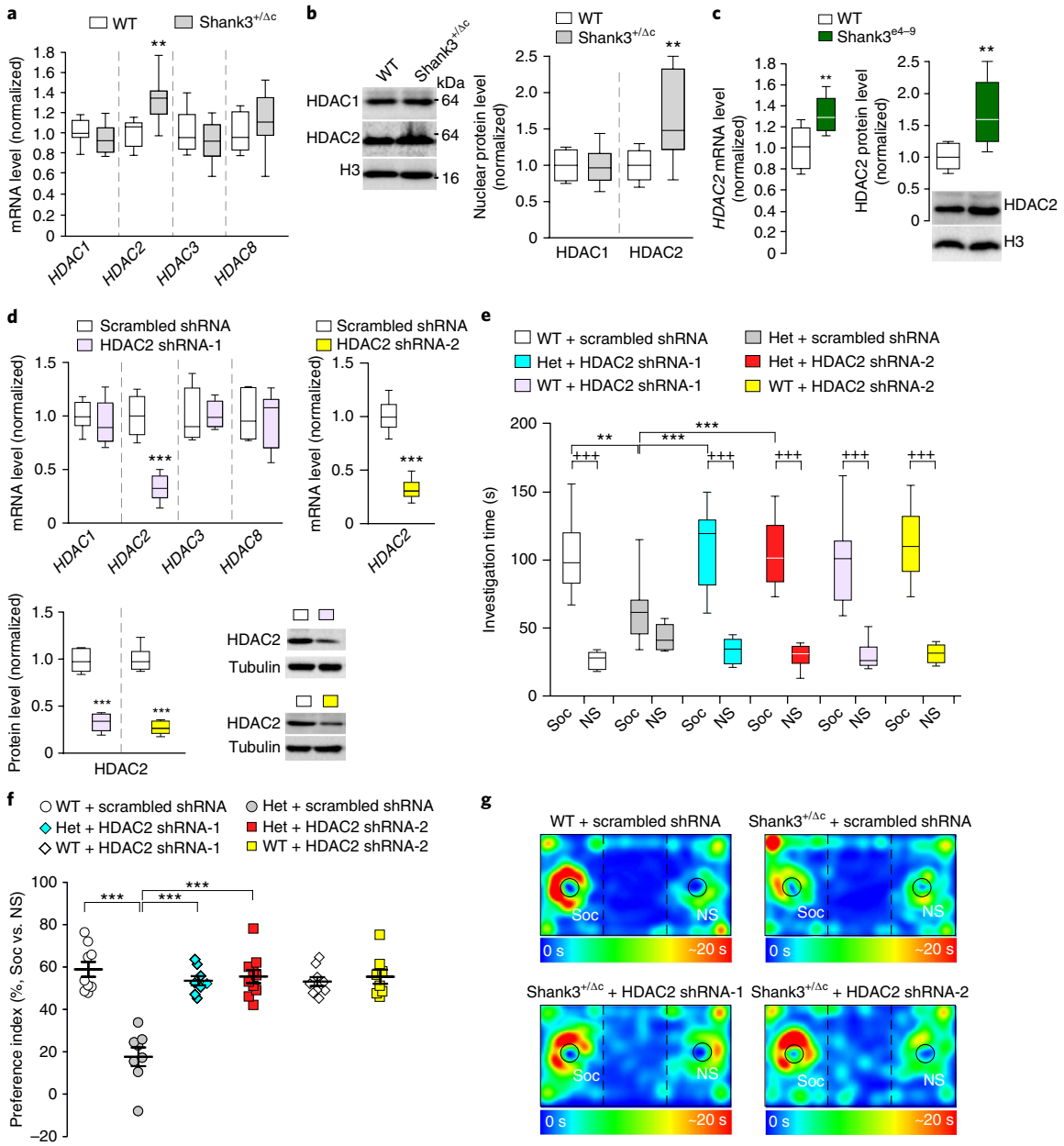

Fig. 3 | *Shank3* deficiency induces HDAC2 upregulation, and *HDAC2* knockdown in PFC rescues autism-like social deficits. a, Quantitative real-time (RT)-PCR data on mRNA levels of class I *HDAC* family members (*HDAC1*, *HDAC2*, *HDAC3*, *HDAC8*) in PFC from WT and Shank3$^{+/\Delta C}$ mice ($t_{16}=3.75$, $^{*}P=0.0017$ (*HDAC2*), $n=9$ per group, two-tailed *t* test). **b**, Immunoblots and quantification analysis of the protein levels of HDAC1 and HDAC2 in the nuclear fraction of PFC neurons from WT vs. Shank3$^{+/\Delta C}$ mice ($t_{16}=3.00$, $^{**}P=0.0085$ (HDAC2), $n=9$ per group, two-tailed *t* test). **c**, Quantitative PCR (qPCR) and western blot data showing HDAC2 mRNA and protein levels in PFC from WT and Shank3^{e4-9} mice ($t_{14}=3.24$, $^{**}P=0.006$ (mRNA), $n=8$ per group; $t_{16}=3.79$, $^{**}P=0.0016$ (protein), $n=9$ per group, two-tailed *t* test). **d**, qPCR and western blot data showing HDAC2 mRNA and protein levels in PFC infected with one of the two different HDAC2 shRNA lentiviruses or a scrambled shRNA lentivirus (shRNA-1: $t_{10}=7.28$, $^{***}P<0.0001$ (*HDAC2* mRNA), $n=6$ per group; $t_{10}=10.84$, $^{***}P<0.0001$ (HDAC2 protein), $n=6$ per group; shRNA-2: $t_{14}=11.33$, $^{***}P<0.0001$ (*HDAC2* mRNA), $n=8$ per group; $t_{10}=12.47$, $^{***}P<0.0001$ (HDAC2 protein), $n=6$ per group, two-tailed *t* test). **e**,**f**, Plots showing the time spent investigating either the social (Soc) or nonsocial (NS) stimulus (**e**; $F_{5,92}=5.1$, $P=0.0004$) and the social preference index (**f**; $F_{2,46}=26.2$, $P<0.0001$) during three-chamber sociability testing of WT or Shank3$^{+/\Delta C}$ mice with PFC injection of one of the two different HDAC2 shRNA lentiviruses or a scrambled shRNA lentivirus ($n=8$–10 per group; $^{+++}P<0.001$, Soc vs. NS, $^{**}P<0.01$, $^{***}P<0.001$, two-way ANOVA). **g**, Representative heat maps of the three-chamber sociability tests of WT or Shank3$^{+/\Delta C}$ mice injected with different viruses. All animals used are males, 5–8 weeks old. Data are presented as medians with interquartile ranges (**a**–**e**) or mean ± s.e.m. (**f**). Each set of experiments was replicated at least three times. See Supplementary Fig. 8 for blot source data.

Romidepsin treatment elevates NMDAR transcription and restores NMDAR function in *Shank3*-deficient mice. We then sought to determine molecular mechanisms downstream of HDAC inhibition that may underlie the amelioration of social deficits. Diminished synaptic signals at glutamatergic synapses are strongly linked to autism-like phenotypes, including social deficits and repetitive behaviors[7–16], making glutamate receptors a potential key target of romidepsin. Quantitative PCR analyses (Fig. 5a) indicated

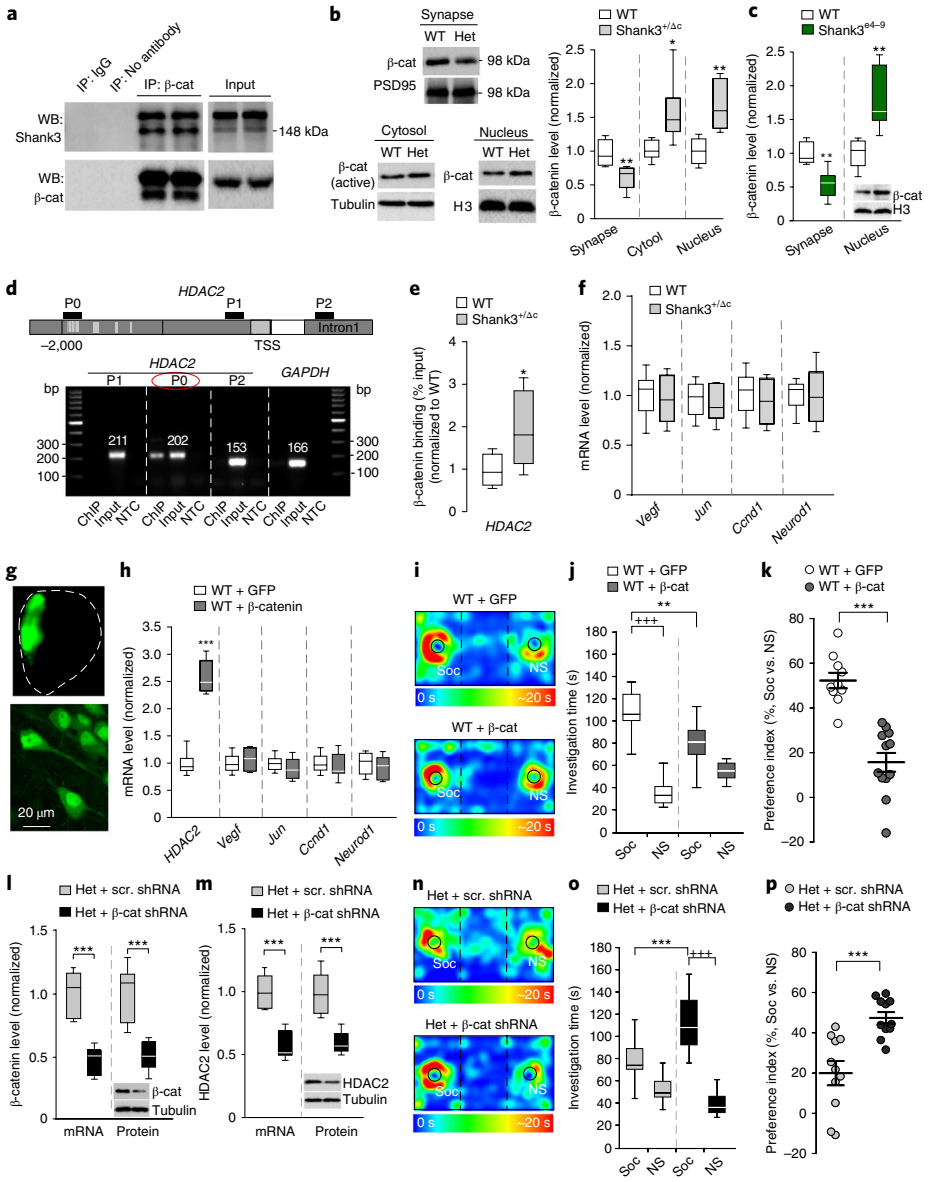

Fig. 4 | β-catenin is nuclear-translocated to activate *HDAC2* transcription in *Shank3*-deficient mice, and manipulation of β-catenin directly affects *HDAC2* transcription and social behaviors. a, Co-immunoprecipitation data from cortical lysates of WT mice showing the specific binding of β-catenin (β-cat) to Shank3. **b**, Immunoblots and quantification analysis of the level of β-catenin in synaptic membrane, cytosol or nuclear fractions of cortical slices from WT and Shank3$^{+/\Delta C}$ (Het) mice ($t_{10}=3.35$, $^{**}P=0.0074$ (synapse), $t_{10}=2.78$, $^{*}P=0.0194$ (cytosol), $t_{10}=4.01$, $^{**}P=0.0025$ (nucleus), $n=6$ per group, two-tailed *t* test). **c**, Quantification analysis of synaptic and nuclear β-catenin levels in cortical slices from WT and Shank3^{e4-9} mice ($t_{10}=4.33$, $^{**}P=0.0015$ (synapse), $t_{10}=3.82$, $^{**}P=0.0034$ (nucleus), $n=6$ per group, two-tailed *t* test). **d**, PCR images showing the ChIP (β-catenin-occupied DNA), input (total DNA) and no-template control (NTC) signals with three primers (P0, P1, P2) designed against different regions of the *HDAC2* gene, including the promoter region containing (P0) or lacking (P1) the TCF–LEF binding motif (labeled with vertical lines) and a downstream intron (P2). TSS, transcriptional start site. *Gapdh* was used as a control. **e**, ChIP assay data showing the binding of β-catenin at *HDAC2* promoter region (containing the TCF–LEF binding motif) in PFC lysates from WT and Shank3$^{+/\Delta C}$ mice ($t_{12}=2.6$, $^{*}P=0.02$, $n=7$ per group, two-tailed *t* test). **f**, Quantitative RT-PCR data on the mRNA level of other β-catenin target genes (*Vegf*, *Jun*, *Ccnd1* and *Neurod1*) in PFC from WT and Shank3$^{+/\Delta C}$ mice ($n=8$ per group). **g**, Images showing the β-catenin (GFP-tagged) adenovirus-infected medial PFC region (top) and PFC neurons (bottom). **h**, qPCR data on the mRNA level of *HDAC2* and other β-catenin target genes in PFC of WT mice with the overexpression of GFP-tagged β-catenin ($n=10$) or GFP control ($n=8$; $t_{16}=13.44$, $^{***}P<0.0001$ (*HDAC2*), two-tailed *t* test). **i**–**k**, Representative heat maps (**i**), plots of social interaction time (**j**) and social preference (**k**) in three-chamber sociability tests of WT mice with overexpression of β-catenin ($n=12$) or GFP controls ($n=10$) in PFC (**j**: $F_{1,40}=20.5$, $P<0.0001$; $^{+++}P<0.001$ (Soc vs. NS), $^{**}P<0.01$ (GFP vs. β-catenin), two-way ANOVA; **k**: $t_{20}=6.4$, $^{***}P<0.0001$, two-tailed *t* test). **l**,**m**, qPCR and western blot data showing mRNA and protein levels of β-catenin (**l**) and HDAC2 (**m**) in Shank3$^{+/\Delta C}$ mice with stereotaxic injection of β-catenin shRNA or a scrambled (scr.) shRNA lentivirus into the PFC (**l**: $t_{10}=6.47$, $^{***}P<0.0001$ (β-*catenin* mRNA); $t_{10}=4.88$, $^{***}P=0.0006$ (β-catenin protein); **m**: $t_{10}=6.20$, $^{***}P=0.0001$ (*HDAC2* mRNA); $t_{10}=5.05$, $^{***}P=0.0005$ (HDAC2 protein), $n=6$ per group, two-tailed *t* test). **n**–**p**, Representative heat maps (**n**), plots of social interaction time (**o**) and social preference (**p**) in three-chamber sociability tests of Shank3$^{+/\Delta C}$ mice injected with β-catenin shRNA ($n=11$) or a scrambled shRNA ($n=11$) lentivirus into the PFC (**o**: $F_{1,40}=15.0$, $P=0.0004$; $^{+++}P<0.001$ (Soc vs. NS), $^{***}P<0.001$ (β-catenin shRNA vs. scrambled shRNA), two-way ANOVA; **p**: $t_{20}=4.36$, $^{***}P=0.0003$, two-tailed *t* test). All animals used are males, 5–8 weeks old. Data are presented as medians with interquartile ranges (**b**,**c**,**e**,**f**,**h**,**j**,**l**,**m**,**o**) or mean ± s.e.m. (**k**,**p**). Each set of experiments was replicated at least three times. See Supplementary Fig. 8 for blot source data.

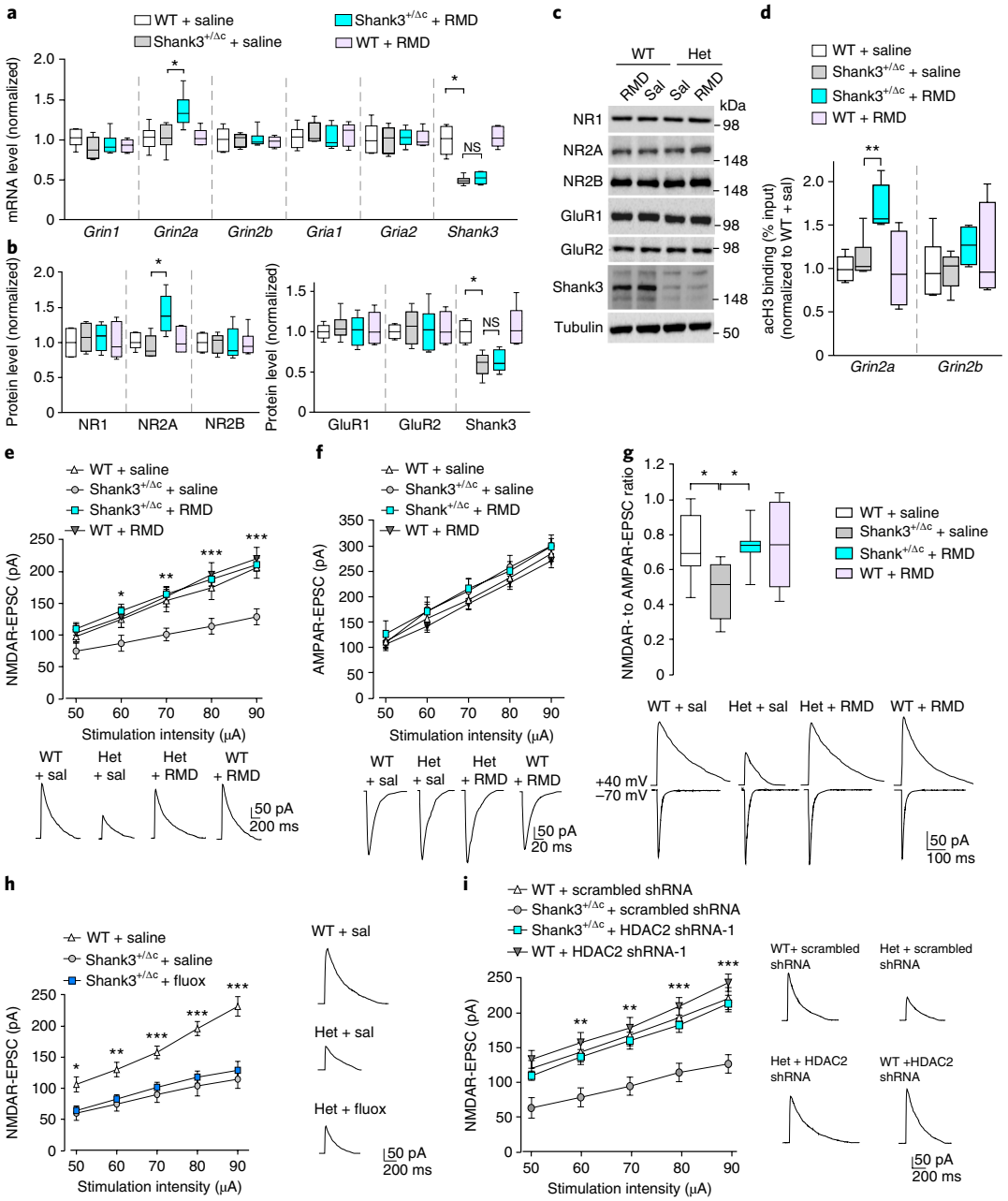

Fig. 5 | Romidepsin treatment increases *Grin2a* transcription and histone acetylation and restores NMDAR synaptic function in PFC of *Shank3*-deficient mice. a, Quantitative RT-PCR data on the mRNA levels of NMDAR and AMPAR subunits and Shank3 in PFC slices from saline-injected WT ($n=8$), saline-injected Shank3$^{+/\Delta C}$ ($n=8$), romidepsin (RMD, 0.25 mg/kg, 3×)-treated Shank3$^{+/\Delta C}$ ($n=10$) and RMD-treated WT ($n=6$) mice ($F_{1,28(\text{treatment})}=5.96$, $P=0.021$ (*Grin2a*); $F_{1,28(\text{treatment})}=0.52$, $P=0.48$ (*Shank3*); $^{*}P<0.05$; ns, not significant, two-way ANOVA). **b**,**c**, Quantification analysis and representative immunoblots of the protein levels of NMDAR and AMPAR subunits and Shank3 in PFC slices from WT or Shank3$^{+/\Delta C}$ mice injected with saline or RMD ($F_{1,20(\text{treatment})}=5.58$, $P=0.030$ (Grin2a); $F_{1,20(\text{treatment})}=0.62$, $P=0.44$ (Shank3); $^{*}P<0.05$, two-way ANOVA, $n=6$ per group). **d**, ChIP assay data showing the acetylated histone H3 (acH3) level at *Grin2a* and *Grin2b* promoter regions in PFC lysates from saline-injected WT ($n=6$), saline-injected Shank3$^{+/\Delta C}$ ($n=6$), RMD-treated Shank3$^{+/\Delta C}$ ($n=6$) and RMD-treated WT ($n=4$) mice ($F_{1,18(\text{treatment})}=5.88$, $P=0.026$ (*Grin2a*); $^{**}P<0.01$, two-way ANOVA). **e**,**f**, Top: input–output curves of NMDAR-EPSC (**e**) and AMPAR-EPSC (**f**) in PFC pyramidal neurons from WT vs. Shank3$^{+/\Delta C}$ mice treated with romidepsin or saline ($n=16$ cells from 4 mice per group). Recordings were performed 4–5 d postinjection ($^{*}P<0.05$, $^{**}P<0.01$, $^{***}P<0.001$ (Shank3$^{+/\Delta C}$ + RMD vs. Shank3$^{+/\Delta C}$ + saline), two-way repeated-measures ANOVA). Bottom: representative NMDAR- and AMPAR-EPSC traces. **g**, Box plots showing the ratio of NMDAR-EPSC to AMPAR-EPSC in PFC pyramidal neurons from WT vs. Shank3$^{+/\Delta C}$ mice treated with RMD or saline ($F_{1,36}=4.8$, $P=0.036$; $^{*}P<0.05$, two-way ANOVA, $n=10$ cells from 3 mice per group). **h**, Left: input–output curves of NMDAR-EPSC in Shank3$^{+/\Delta C}$ mice treated with fluoxetine (fluox; 5 mg/kg, i.p., 14×). Right: representative NMDAR-EPSC traces ($^{*}P<0.05$, $^{**}P<0.01$, $^{***}P<0.001$ (Shank3$^{+/\Delta C}$ + fluoxetine vs. WT + saline), two-way repeated-measures ANOVA), $n=12$ cells from 3 mice per group). **i**, Left: input–output curves of NMDAR-EPSC in PFC pyramidal neurons of WT or Shank3$^{+/\Delta C}$ mice with PFC injection of an HDAC2 shRNA or a scrambled control shRNA lentivirus ($^{**}P<0.01$, $^{***}P<0.001$ (Shank3$^{+/\Delta C}$ + HDAC2 shRNA vs. Shank3$^{+/\Delta C}$ + scrambled shRNA), two-way repeated-measures ANOVA, $n=12$ cells from 3 mice per group). All animals used are males, 5–6 weeks old. Data are presented as medians with interquartile ranges (**a**–**c**,**g**) or mean ± s.e.m. (**e**,**f**,**h**,**i**). Each set of experiments was replicated at least three times. See Supplementary Fig. 9 for blot source data.

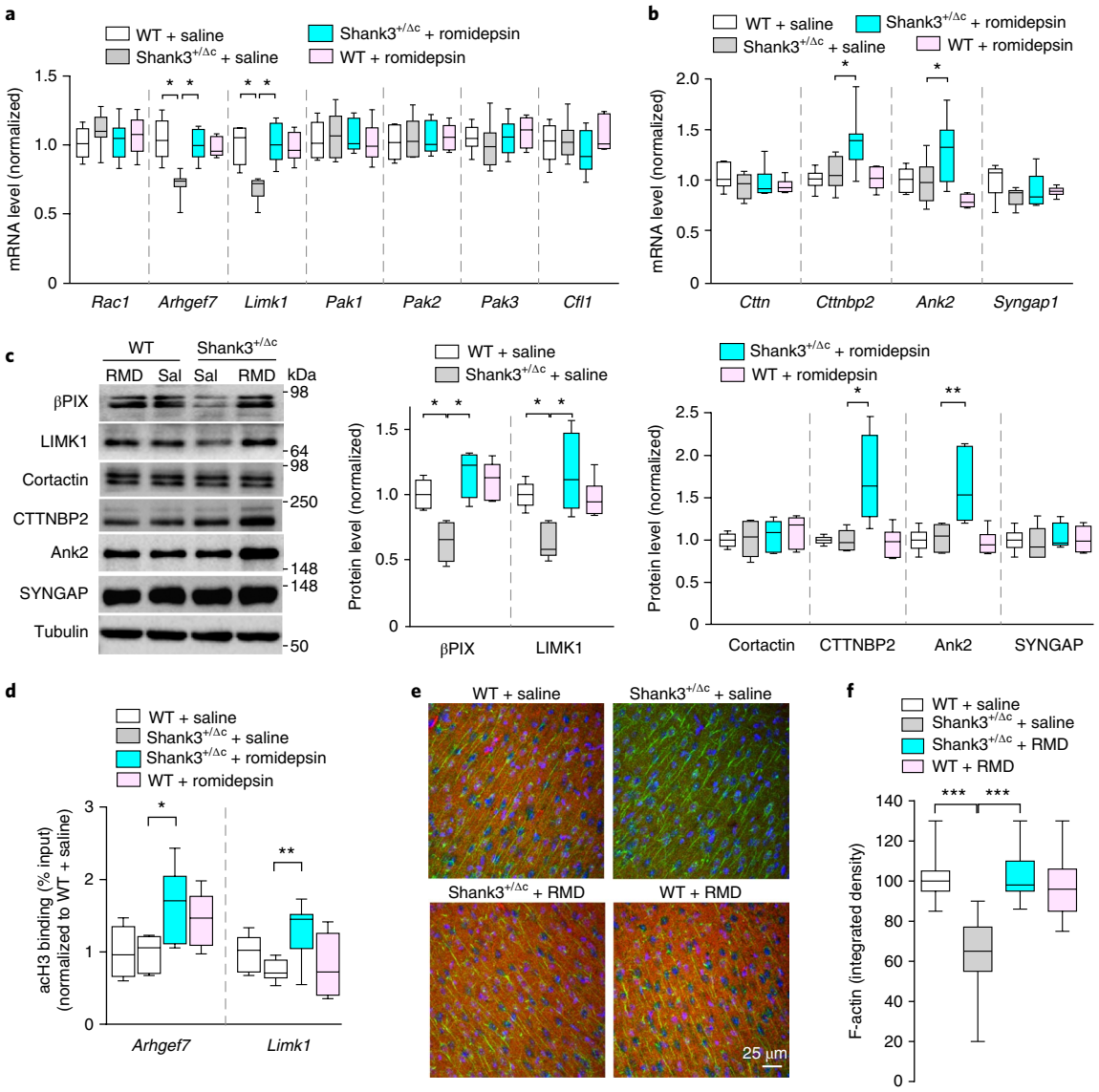

Fig. 6 | Romidepsin treatment elevates the expression of actin regulators and normalizes actin filaments in PFC of *Shank3*-deficient mice. a,**b**, Quantitative RT-PCR data on the mRNA level of actin regulators in the Rac1 signaling pathway (**a**) and those identified as ASD risk factors (**b**) in PFC slices from saline-injected WT ($n=8$), saline-injected Shank3$^{+/\Delta C}$ ($n=8$), romidepsin (RMD, 0.25 mg/kg, 3×)-treated Shank3$^{+/\Delta C}$ ($n=10$) and RMD-treated WT ($n=6$) mice ($F_{1,28}=6.42$, $P=0.017$ (*Arhgef7*); $F_{1,28}=8.04$, $P=0.0086$ (*Limk1*); $F_{1,28(\text{treatment})}=5.93$, $P=0.022$ (*Cttnbp2*); $F_{1,28(\text{treatment})}=7.71$, $P=0.01$ (*Ank2*); $^{*}P<0.05$, two-way ANOVA). **c**, Immunoblots and quantification analysis of the protein level of selected actin regulators in PFC slices from WT or Shank3$^{+/\Delta C}$ mice injected with saline or RMD ($F_{1,20}=6.87$, $P=0.016$ (βPIX); $F_{1,20}=10.87$, $P=0.0036$ (LIMK1); $F_{1,20(\text{treatment})}=4.97$, $P=0.038$ (CTTNBP2); $F_{1,20(\text{treatment})}=9.12$, $P=0.0068$ (ANK2); $^{*}P<0.05$, $^{**}P<0.01$, two-way ANOVA, $n=6$ per group). **d**, ChIP assay data showing the acetylated histone H3 level at *Arhgef7*- and *Limk1*-promoter regions in PFC lysates from saline-injected WT ($n=8$), saline-injected Shank3$^{+/\Delta C}$ ($n=7$), RMD-treated Shank3$^{+/\Delta C}$ ($n=9$) and RMD-treated WT ($n=6$) mice ($F_{1,26(\text{treatment})}=14.6$, $P=0.0007$ (*Arhgef7*); $F_{1,26}=10.0$, $P=0.004$ (*Limk1*); $^{*}P<0.05$, $^{**}P<0.01$, two-way ANOVA). **e**, Merged confocal images (40×) of F-actin (phalloidin, red) co-stained with PSD-95 (green) and DAPI (blue) in PFC slices of WT and Shank3$^{+/\Delta C}$ mice treated with RMD or saline. Immunohistochemistry was performed 4–5 d postinjection. **f**, Quantification of F-actin (integrated densities) in PFC slices of different animal groups ($F_{1,104}=54.49$, $P<0.0001$; $^{***}P<0.001$, two-way ANOVA, $n=27$ images from 3 mice per group). All animals used are males, 5–6 weeks old. Data are presented as medians with interquartile ranges (**a**–**d**,**f**). Each set of experiments was replicated at least three times. See Supplementary Fig. 9 for blot source data.

that in Shank3$^{+/\Delta C}$ mice treated with romidepsin, the mRNA level of *Grin2a* (encoding the NMDAR NR2A subunit) was significantly elevated, while the transcripts encoding other NMDAR subunits (*Grin1*, *Grin2b*) or AMPA-receptor subunits (*Gria1*, *Gria2*) were not significantly changed. Consistently, romidepsin significantly increased the expression of the NR2A subunit, but not other glutamate receptor subunits. The reduced Shank3 mRNA and protein levels in Shank3$^{+/\Delta C}$ mice were not restored by romidepsin treatment (Fig. 5b,c).

The transcriptional increase of *Grin2a* by romidepsin prompted us to investigate whether histone acetylation of NMDA receptors was altered by this HDAC inhibitor. To test this, we performed ChIP assays to examine the histone acetylation at *Grin2a* and *Grin2b* promoters in PFC neurons. H3 acetylation (Supplementary Fig. 3) was identified at the *Grin2a* proximal promoter region (~200 bp from transcription start site or TSS) and *Grin2b* promoter region (~700 bp from TSS). As shown in Fig. 5d, romidepsin treatment significantly increased H3 acetylation at the *Grin2a* promoter in

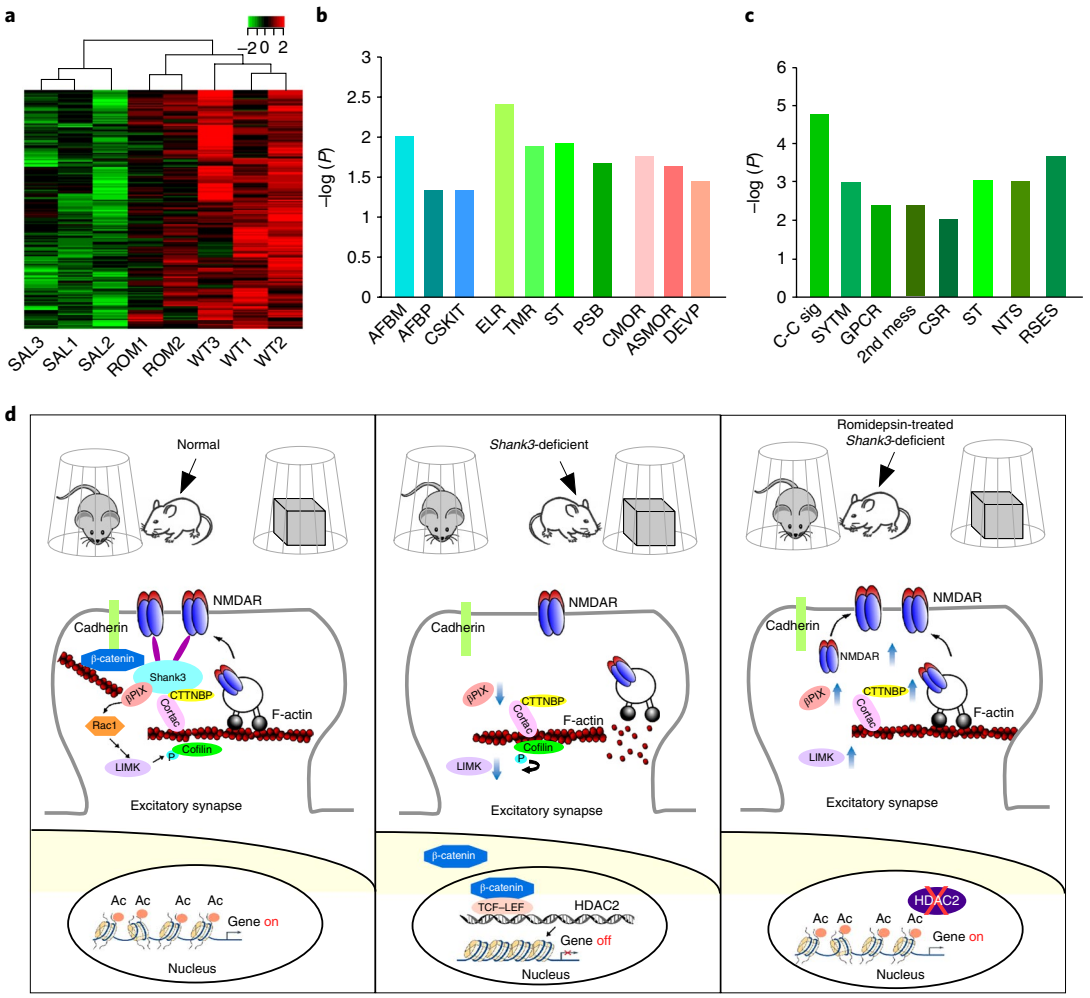

Fig. 7 | Romidepsin treatment induces genome-wide restoration or elevation of genes involved in neural signaling in PFC of *Shank3*-deficient mice. a, Heat map representing expression (row *z*-score) of 187 genes that were downregulated in saline-treated Shank3$^{+/\Delta C}$ mice (SAL, $n=3$) and normalized in romidepsin (RMD, 0.25 mg/kg, 3×)-treated Shank3$^{+/\Delta C}$ mice (ROM, $n=2$), compared to WT mice ($n=3$). All animals used are males, 5–6 weeks old. **b**, Enrichment analysis using gene sets derived from the Biological Process Ontology for the 187 genes that were suppressed in Shank3$^{+/\Delta C}$ mice and restored by romidepsin treatment. AFBM, actin filament-based movement; AFBP, actin filament-based process; CSKIT, cytoskeleton-dependent intracellular transport; ELR, enzyme-linked receptor protein signaling pathway; TMR, transmembrane receptor protein signaling pathway; ST, signal transduction; PSB, regulation of protein stability; CMOR, regulation of cell morphogenesis; ASMOR, anatomical structure morphogenesis; DEVP, regulation of developmental process. **c**, Enrichment analysis for the 41 genes that were unchanged in Shank3$^{+/\Delta C}$ mice but were elevated by romidepsin treatment. C-C sig, cell–cell signaling; SYTM, synaptic transmission; GPCR, G-protein-coupled receptor protein signaling pathway; 2nd mess, second-messenger signaling; CSR, cell surface receptor-linked signal transduction; NTS, neurotransmitter secretion; RSES, response to external stimulus. **d**, Schematic showing the potential mechanism underlying the therapeutic effect of romidepsin in *Shank3*-deficient mice. Normally, Shank3 crosslinks NMDARs to actin cytoskeleton and binds to the adhesive junction-associated protein β-catenin. Loss of Shank3 leads to the translocation of β-catenin from synapses to nucleus, inducing the upregulation of HDAC2 and chromatin remodeling. The ensuing transcriptional suppression of actin regulators results in the disruption of actin filaments and the synaptic delivery of NMDARs. Treatment with romidepsin restores or elevates many target genes, including NMDAR subunits, key actin regulators and others involved in neuronal signaling, leading to the normalization of actin cytoskeleton and NMDAR synaptic function. Consequently, the autism-like social deficits are rescued.

Shank3$^{+/\Delta C}$ mice. No significant effect of romidepsin on H3 acetylation at *Grin2b* promoter was observed. These data suggest that romidepsin treatment of Shank3$^{+/\Delta C}$ mice elevates *Grin2a* gene expression by enhancing its histone acetylation.

The upregulation of *Grin2a* transcription by romidepsin could lead to elevated NMDAR function in Shank3$^{+/\Delta C}$ mice. Thus, we performed electrophysiological experiments to record NMDAR-mediated excitatory postsynaptic currents (EPSC) 3–5 d after romidepsin treatment in layer V PFC pyramidal neurons, which exhibit the clearest deficits in the brains of children with autism[33]. As shown in Fig. 5e, the amplitudes of NMDAR-EPSC induced by a series of stimulus intensities were markedly reduced in saline-injected Shank3$^{+/\Delta C}$ mice, compared to saline-injected WT mice. A strong recovery of the input–output curves of NMDAR-EPSC was observed in PFC neurons of Shank3$^{+/\Delta C}$ mice with romidepsin treatment. AMPA-receptor (AMPAR)-ESPC were unchanged in Shank3$^{+/\Delta C}$ mice treated with romidepsin or saline (Fig. 5f). The NMDAR- to AMPAR-EPSC ratio was significantly reduced in Shank3$^{+/\Delta C}$ mice and was also restored by romidepsin treatment (Fig. 5g). In contrast, fluoxetine treatment (10 mg/kg, i.p. 14×) failed to elevate NMDAR-EPSC in Shank3$^{+/\Delta C}$ mice (Fig. 5h). Moreover, in PFC pyramidal neurons of HDAC2 shRNA-injected

Shank3$^{+/\Delta C}$ mice, diminished NMDAR were significantly restored (Fig. 5i). The romidepsin-induced rescue of NMDAR-EPSC, as well as the romidepsin-induced normalization of global H3 acetylation, could be observed 16–18 d post-treatment, but not 30–32 d post-treatment (Supplementary Fig. 4), consistent with the therapeutic time window of romidepsin on behaviors (Fig. 1e). These results suggest that the recovery of NMDAR function in PFC may underlie the rescue of social deficits in *Shank3*-deficient mice with HDAC2 inhibition or knockdown.

Romidepsin treatment elevates the transcription of actin regulators and restores F-actin in *Shank3*-deficient mice. To determine the potential existence of other molecular targets of romidepsin, we focused on various actin regulators in the 'Shank3 interactome'[34] that could regulate synaptic structure and NMDAR trafficking[12]. Enriched mutations in genes regulating actin filament networks have been identified in genetic analyses of ASD patients[19,35], suggesting that actin dysregulation at glutamatergic synapses is a potential pathophysiological mechanism. It has been found that the Rac1–LIMK–PAK–cofilin signaling pathway is disrupted in *Shank3*-deficient mice, leading to F-actin dysregulation[12], so we first examined the mRNA levels of these genes. As shown in Fig. 6a, *Arhgef7*, which encodes βPIX, the guanine nucleotide exchange factor for Rac1 and a Shank-interacting protein at excitatory synaptic sites[36], was significantly lost in Shank3$^{+/\Delta C}$ mice, and romidepsin treatment rescued *Arhgef7* gene transcription. The significantly decreased *Limk1*, which encodes a major Rac1 downstream target controlling cofilin activity, was also restored by romidepsin treatment of *Shank3*-deficient mice. The mRNA levels of *Rac1*, *Pak1/2/3* and *Cfl1* (encoding cofilin) were largely unchanged.

The mRNA levels of several other Shank3-interacting actin regulators that have been identified as ASD risk factors[19] were also examined. As shown in Fig. 6b, *Cttnbp2*, which encodes a protein binding to cortactin (an F-actin- and Shank3-interacting protein), was upregulated in Shank3$^{+/\Delta C}$ mice treated with romidepsin. A similar upregulation was found in *Ank2* (encoding Ankyrin2), while *Cttn* (encoding cortactin) and *Syngap1* mRNAs showed no change.

We further examined the alteration of protein levels of these actin regulators. As shown in Fig. 6c, the diminished expression of βPIX and LIMK1 in *Shank3*-deficient mice was restored by romidepsin treatment. Moreover, romidepsin significantly increased the protein level of CTTNBP2 and Ank2 without altering cortactin or SYNGAP.

To test whether the transcriptional increase of actin regulators by romidepsin could be due to increased histone acetylation, we performed ChIP assays to examine the histone acetylation at *Arhgef7* and *Limk1* promoters in PFC neurons. H3 acetylation (Supplementary Fig. 5) was identified at the *Arhgef7* promoter region (~800 bp from TSS) and *Limk1* promoter region (~500 bp from TSS). As shown in Fig. 6d, romidepsin treatment of Shank3$^{+/\Delta C}$ mice significantly increased the enrichment of H3 acetylation at *Arhgef7* promoter and *Limk1* promoter.

Romidepsin-induced upregulation of key actin regulators in the Shank3 interactome may help to restore and maintain the integrity of actin cytoskeleton at synapses. To test this, we performed immunostaining with phalloidin to directly visualize F-actin. As shown in Fig. 6e,f and Supplementary Fig. 6, compared to WT mice, Shank3$^{+/\Delta C}$ mice (saline-injected) had a significant decrease of F-actin expression in PFC slices, and romidepsin treatment restored cortical actin filaments to the normal level. Expression of PSD-95 in PFC of Shank3$^{+/\Delta C}$ mice was unchanged by romidepsin treatment. The normalization of actin filaments may facilitate actin-based NMDAR membrane delivery.

To examine the region-specificity of romidepsin-induced gene expression changes, we performed qPCR profiling in several other brain regions and peripheral organs. In contrast to what was found in PFC, the levels of mRNA encoding NMDAR subunits (*Grin1*, *Grin2a* and *Grin2b*) and actin regulators (*Arhgef7* and *Limk1*) in dorsal striatum, ventral tegmental area, kidney and heart of Shank3$^{+/\Delta C}$ mice were not significantly altered by romidepsin treatment (Supplementary Fig. 7).

Romidepsin treatment induces genome-wide restoration or elevation of expression of genes involved in neural signaling in PFC of *Shank3*-deficient mice. Finally, to determine whether HDAC inhibition has genome-wide effects on gene expression, we used RNA sequencing to analyze the mRNA profile in PFC of WT and Shank3$^{+/\Delta C}$ mice treated with romidepsin or saline control. We mapped the sequences to 24,420 mouse genes. Compared to WT mice, in saline-treated Shank3$^{+/\Delta C}$ mice 365 genes showed a change in expression values of at least 1.2-fold and $P \leq 0.01$ (213 downregulated, 152 upregulated). In romidepsin-treated Shank3$^{+/\Delta C}$ mice, many of the downregulated genes ($n = 187$ genes) were normalized to control values (Supplementary Table 1). The heat map generated with the expression values for the 187 restored genes showed that the saline-treated Shank3$^{+/\Delta C}$ samples clustered together and separated from the WT samples. Moreover, romidepsin-treated Shank3$^{+/\Delta C}$ samples were closer to those from WT than to the saline-treated Shank3$^{+/\Delta C}$ samples (Fig. 7a). Further analysis of the romidepsin-restored genes revealed enrichment in actin cytoskeleton-mediated transport, signal transduction pathways and developmental processes (Fig. 7b). In addition, romidepsin treatment increased the expression of 41 genes that were unchanged in Shank3$^{+/\Delta C}$ samples (Supplementary Table 2), which were enriched in cell–cell signaling, synaptic transmission and neurotransmitter secretion (Fig. 7c). These results suggest that romidepsin treatment can rescue or elevate the expression of many genes involved in neural signaling in *Shank3*-deficient mice, which may collectively contribute to its therapeutic effects on behavioral deficits (Fig. 7d).

Discussion

Here we show that *Shank3*-deficient mice exhibit an abnormally low level of histone acetylation resulting from *HDAC2* upregulation in the PFC. Brief treatment with a low dose of romidepsin, a potent class I HDAC inhibitor, leads to robust and long-lasting rescue of social deficits, a core symptom of ASD. This effect of romidepsin was unique, as many of the pharmacological agents currently used in psychiatric practice, including fluoxetine, clozapine, valproic acid, risperidone and aripiprazole, all fail to profoundly and persistently improve social behaviors in the *Shank3* model. This low-dose romidepsin treatment does not induce locomotor deficits, changes in anxiety-like behavior or neuronal loss in young animals. The most effective therapeutic window of romidepsin is the juvenile to late-adolescent period, which is a critical developmental stage for social and communication skills. The sustained rescue effect on social deficits of a single-round administration of romidepsin in young *Shank3*-deficient mice is promising, but it is limited by the lack of chronic effects in adulthood with repeated administrations. Using romidepsin as a tool compound to interrogate the biology of *Shank3* deficiency, we demonstrated how aberrations in synaptic, transcriptional and epigenetic pathways, all of which have been implicated in autism[19–21], are interconnected.

One critical question is the molecular mechanism underlying the epigenetic aberrations in *Shank3* deficiency models. We found that *Shank3* deficiency induced nuclear translocation of its binding partner at synapses, β-catenin. *HDAC2* transcription is upregulated in *Shank3*-deficient mice, which is associated with the increased enrichment of β-catenin at the *HDAC2* promoter region containing TCF–LEF binding elements. Direct overexpression of β-catenin in PFC of WT mice leads to the upregulation of *HDAC2* transcription, and knockdown of β-catenin in PFC of *Shank3*-deficient mice leads to the reduction of *HDAC2* transcription, further suggesting that

HDAC2 is a target gene of β-catenin. Moreover, social deficits are rescued by inhibition of HDAC2, knockdown of HDAC2 or knockdown of β-catenin in PFC of *Shank3*-deficient mice, and they are induced by elevating β-catenin expression in PFC of WT mice. These bidirectional lines of evidence strongly suggest that β-catenin–HDAC2 plays a causal role in social deficits of *Shank3*-deficiency models and the therapeutic effect of romidepsin.

Finding potential targets downstream of HDAC inhibition involved in the amelioration of social deficits is another challenge. Aberrant synaptic function resulting from genetic mutations is thought to be a major pathogenic factor in ASD[18–20,37,38]. The behavioral abnormalities exhibited in *Shank3*-deficient mice have been attributed to the alteration of glutamatergic synapses[7–16]. In particular, aberrations in NMDARs, a Shank3-associated key synaptic protein[2] controlling neural development and synaptic plasticity underlying cognitive processes, are strongly linked to social deficits[12,39–41]. Previous studies demonstrate that the *Shank3*-deficiency-induced NMDAR hypofunction is due to the loss of actin-based synaptic delivery of NMDARs because of the reduced Rac1–PAK–cofilin signaling[12,42]. Romidepsin treatment of *Shank3*-deficient mice normalizes the aberrant histone acetylation and elevates the transcription of many downstream target genes, including NMDAR subunits and key actin regulators, leading to the restoration of synaptic NMDAR function and F-actin in PFC neurons. These results are also supported by our RNA sequencing data. The majority of the 213 downregulated genes in *Shank3*-deficient mice was restored by romidepsin treatment, and these genes are highly enriched in actin cytoskeleton-mediated transport, signal transduction pathways and developmental processes. The reversal of the haploinsufficiency of a number of genes identified as key ASD risk factors provides a potential mechanism for the romidepsin-induced rescue of social deficits in *Shank3*-deficient mouse models.

Methods

Methods, including statements of data availability and any associated accession codes and references, are available at https://doi.org/10.1038/s41593-018-0110-8.

Received: 18 December 2017; Accepted: 25 January 2018;
Published online: 12 March 2018

References

1. Silverman, J. L., Yang, M., Lord, C. & Crawley, J. N. Behavioural phenotyping assays for mouse models of autism. *Nat. Rev. Neurosci.* **11**, 490–502 (2010).
2. Naisbitt, S. et al. Shank, a novel family of postsynaptic density proteins that binds to the NMDA receptor/PSD-95/GKAP complex and cortactin. *Neuron* **23**, 569–582 (1999).
3. Bonaglia, M. C. et al. Disruption of the *ProSAP2* gene in a t(12;22)(q24.1;q13.3) is associated with the 22q13.3 deletion syndrome. *Am. J. Hum. Genet.* **69**, 261–268 (2001).
4. Durand, C. M. et al. Mutations in the gene encoding the synaptic scaffolding protein SHANK3 are associated with autism spectrum disorders. *Nat. Genet.* **39**, 25–27 (2007).
5. Betancur, C. & Buxbaum, J. D. *SHANK3* haploinsufficiency: a "common" but underdiagnosed highly penetrant monogenic cause of autism spectrum disorders. *Mol. Autism* **4**, 17 (2013).
6. Leblond, C. S. et al. Meta-analysis of *SHANK* mutations in autism spectrum disorders: a gradient of severity in cognitive impairments. *PLoS Genet.* **10**, e1004580 (2014).
7. Jiang, Y. H. & Ehlers, M. D. Modeling autism by *SHANK* gene mutations in mice. *Neuron* **78**, 8–27 (2013).
8. Bozdagi, O. et al. Haploinsufficiency of the autism-associated *Shank3* gene leads to deficits in synaptic function, social interaction, and social communication. *Mol. Autism* **1**, 15 (2010).
9. Peça, J. et al. *Shank3* mutant mice display autistic-like behaviours and striatal dysfunction. *Nature* **472**, 437–442 (2011).
10. Wang, X. et al. Synaptic dysfunction and abnormal behaviors in mice lacking major isoforms of Shank3. *Hum. Mol. Genet.* **20**, 3093–3108 (2011).
11. Kouser, M. et al. Loss of predominant Shank3 isoforms results in hippocampus-dependent impairments in behavior and synaptic transmission. *J. Neurosci.* **33**, 18448–18468 (2013).
12. Duffney, L. J. et al. Autism-like deficits in Shank3-deficient mice are rescued by targeting actin regulators. *Cell Rep.* **11**, 1400–1413 (2015).
13. Wang, X. et al. Altered mGluR5-Homer scaffolds and corticostriatal connectivity in a *Shank3* complete knockout model of autism. *Nat. Commun.* **7**, 11459 (2016).
14. Bidinosti, M. et al. CLK2 inhibition ameliorates autistic features associated with SHANK3 deficiency. *Science* **351**, 1199–1203 (2016).
15. Speed, H. E. et al. Autism-associated insertion mutation (InsG) of SHANK3 exon 21 causes impaired synaptic transmission and behavioral deficits. *J. Neurosci.* **35**, 9648–9665 (2015).
16. Jaramillo, T. C. et al. Altered striatal synaptic function and abnormal behaviour in *Shank3* Exon4-9 deletion mouse model of autism. *Autism Res.* **9**, 350–375 (2016).
17. Amodio, D. M. & Frith, C. D. Meeting of minds: the medial frontal cortex and social cognition. *Nat. Rev. Neurosci.* **7**, 268–277 (2006).
18. Delorme, R. et al. Progress toward treatments for synaptic defects in autism. *Nat. Med.* **19**, 685–694 (2013).
19. De Rubeis, S. et al. Synaptic, transcriptional and chromatin genes disrupted in autism. *Nature* **515**, 209–215 (2014).
20. Chen, J. A., Peñagarikano, O., Belgard, T. G., Swarup, V. & Geschwind, D. H. The emerging picture of autism spectrum disorder: genetics and pathology. *Annu. Rev. Pathol.* **10**, 111–144 (2015).
21. Crawley, J. N., Heyer, W. D. & LaSalle, J. M. Autism and cancer share risk genes, pathways, and drug targets. *Trends Genet.* **32**, 139–146 (2016).
22. Guan, J. S. et al. HDAC2 negatively regulates memory formation and synaptic plasticity. *Nature* **459**, 55–60 (2009).
23. Fischer, A., Sananbenesi, F., Mungenast, A. & Tsai, L. H. Targeting the correct HDAC(s) to treat cognitive disorders. *Trends Pharmacol. Sci.* **31**, 605–617 (2010).
24. Tsankova, N., Renthal, W., Kumar, A. & Nestler, E. J. Epigenetic regulation in psychiatric disorders. *Nat. Rev. Neurosci.* **8**, 355–367 (2007).
25. Grayson, D. R., Kundakovic, M. & Sharma, R. P. Is there a future for histone deacetylase inhibitors in the pharmacotherapy of psychiatric disorders? *Mol. Pharmacol.* **77**, 126–135 (2010).
26. Klimek, V. M. et al. Tolerability, pharmacodynamics, and pharmacokinetics studies of depsipeptide (romidepsin) in patients with acute myelogenous leukemia or advanced myelodysplastic syndromes. *Clin. Cancer Res.* **14**, 826–832 (2008).
27. Piekarz, R. L. et al. Phase II multi-institutional trial of the histone deacetylase inhibitor romidepsin as monotherapy for patients with cutaneous T-cell lymphoma. *J. Clin. Oncol.* **27**, 5410–5417 (2009).
28. Fraczek, J., Vanhaecke, T. & Rogiers, V. Toxicological and metabolic considerations for histone deacetylase inhibitors. *Expert Opin. Drug Metab. Toxicol.* **9**, 441–457 (2013).
29. McPheeters, M. L. et al. A systematic review of medical treatments for children with autism spectrum disorders. *Pediatrics* **127**, e1312–e1321 (2011).
30. Valenta, T., Hausmann, G. & Basler, K. The many faces and functions of β-catenin. *EMBO J.* **31**, 2714–2736 (2012).
31. Murase, S., Mosser, E. & Schuman, E. M. Depolarization drives beta-Catenin into neuronal spines promoting changes in synaptic structure and function. *Neuron* **35**, 91–105 (2002).
32. Yu, X. & Malenka, R. C. Beta-catenin is critical for dendritic morphogenesis. *Nat. Neurosci.* **6**, 1169–1177 (2003).
33. Stoner, R. et al. Patches of disorganization in the neocortex of children with autism. *N. Engl. J. Med.* **370**, 1209–1219 (2014).
34. Han, K. et al. *SHANK3* overexpression causes manic-like behaviour with unique pharmacogenetic properties. *Nature* **503**, 72–77 (2013).
35. Gilman, S. R. et al. Rare de novo variants associated with autism implicate a large functional network of genes involved in formation and function of synapses. *Neuron* **70**, 898–907 (2011).
36. Park, E. et al. The Shank family of postsynaptic density proteins interacts with and promotes synaptic accumulation of the beta PIX guanine nucleotide exchange factor for Rac1 and Cdc42. *J. Biol. Chem.* **278**, 19220–19229 (2003).
37. Shcheglovitov, A. et al. SHANK3 and IGF1 restore synaptic deficits in neurons from 22q13 deletion syndrome patients. *Nature* **503**, 267–271 (2013).
38. Ebrahimi-Fakhari, D. & Sahin, M. Autism and the synapse: emerging mechanisms and mechanism-based therapies. *Curr. Opin. Neurol.* **28**, 91–102 (2015).
39. Carlson, G. C. Glutamate receptor dysfunction and drug targets across models of autism spectrum disorders. *Pharmacol. Biochem. Behav.* **100**, 850–854 (2012).
40. Won, H. et al. Autistic-like social behaviour in Shank2-mutant mice improved by restoring NMDA receptor function. *Nature* **486**, 261–265 (2012).

41. Chung, W. et al. Social deficits in IRSp53 mutant mice improved by NMDAR and mGluR5 suppression. *Nat. Neurosci.* **18**, 435–443 (2015).
42. Duffney, L. J. et al. Shank3 deficiency induces NMDA receptor hypofunction via an actin-dependent mechanism. *J. Neurosci.* **33**, 15767–15778 (2013).

Acknowledgements

We thank X.Q. Chen for excellent technical support. This work was supported by the Nancy Lurie Marks Family Foundation and grants from the National Institutes of Health (MH112237, MH108842 and DA037618) to Z.Y. We also thank E.F. Trachtman and the Varanasi family for their donations.

Author contributions

L.Q. performed immunocytochemical and electrophysiological experiments and analyzed data. K.M. performed behavioral tests and analyzed data. L.Q., Z.-J.W., E.M. and J.W. performed biochemical and molecular biological experiments and analyzed data. Z.H. performed bioinformatic analysis. Z.Y. designed experiments, supervised the project and wrote the paper.

Competing interests

The authors declare no competing financial interests.

Additional information

Supplementary information is available for this paper at https://doi.org/10.1038/s41593-018-0110-8.

Correspondence and requests for materials should be addressed to Z.Y.

Methods

Animals and compounds. Mice expressing C-terminal (exon 21)-deleted Shank3 (Jackson Labs, Bar Harbor, ME), which exhibited the significant loss of full-length Shank3 expression, were generated, genotyped and maintained as previously described[11,12]. Since only the hemizygous deletion or loss-of-function mutation in the *Shank3* gene has been linked to human autism and intellectual disability[3,4], heterozygous Shank3$^{+/\Delta C}$ mice (5–8 weeks old, male) and age-matched WT littermates (male) were used in this study. Female Shank3$^{+/\Delta C}$ mice lack the autism-like social deficits, so they were not used.

Shank3^{e4-9} mice with the loss of major isoforms of the *Shank3* gene resulting from the deletion of N-terminal exons 4–9 (a kind gift from Y.-H. Jiang at Duke University School of Medicine) were generated, genotyped and maintained as previously described[10]. Both male and female homozygous Shank3^{e4-9} mice, which exhibit prominent autism-like social preference deficits[10], were used. Similar results were obtained, so results from males and females were pooled together.

Mice of different genotypes were randomly assigned to drug/saline groups. Experiments were carried out by investigators in a blinded fashion (with no prior knowledge of genotypes and treatments). All experiments were performed with the approval of the Institutional Animal Care and Use Committee (IACUC) of the State University of New York at Buffalo. We have complied with all relevant ethical regulations.

Romidepsin (Selleckchem), fluoxetine (NIH), valproic acid (Tocris), aripiprazole (Tocris), risperidone (Tocris) or trichostatin A (Sigma) was prepared by dissolving them in DMSO to make stock solutions and diluting them with 0.9% saline before injections (DMSO concentration of the working solutions: < 0.2%). All tests were performed on various days, as indicated, after the last injection of the compound.

Behavioral testing. *Social preference test.* A three-chamber social-interaction assay was performed to assess social deficits[12]. Briefly, an apparatus (L: 101.6 cm, W: 50.8 cm, H: 50.8 cm) containing three chambers with retractable doorways allowing for access to side chambers was used. The test was composed of two phases with different stimuli in each of the two side chambers. Each stimulus was placed inside a capsule (an inverted pencil cup, D: 10.2 cm, H: 10.5 cm). An upright plastic drinking cup was placed on top of each capsule to prevent the subject mouse from climbing on top. The first phase contained two identical nonsocial stimuli (folded black papers); the second phase contained a nonsocial (NS) stimulus (a wood block) and a social (Soc) stimulus (age- and sex-matched mouse of the same strain). Locations of the NS and Soc stimuli were counterbalanced. Animals were habituated to the three-chamber apparatus 1 d before the initial testing. During habituation, two empty capsules were placed in the side chambers, and animals were allowed to explore for 10 min. During the sociability measurement, different stimuli were placed in the capsules in the side chambers, and the test animal was placed in the center chamber and was free to explore the apparatus for 10 min in each phase. The subject mouse was returned to its home cage during the 5-min intervals between test phases. The chamber was cleaned with 75% ethanol after each phase. Interaction time was counted based on 'investigating' behaviors of the test animal toward each stimulus. In earlier experiments, an experimenter measured the time the test animal spent actively seeking and sniffing the stimulus. In later experiments, a computer running ANY-maze behavior tracking software (Stoelting, Wood Dale, IL) measured the time the test animal spent in close proximity to the capsule (distance of animal head to cup edge: ≤3.5 cm). Data generated manually and automatically were consistent, so they were pooled together. Preference scores were calculated, where time spent with one stimulus was subtracted from the time spent with the other stimulus and divided by the total time spent exploring both stimuli.

Social approach test. The test animal was habituated in an apparatus (L: 67.7 cm, W: 50.8 cm, H: 50.8 cm) containing a capsule (an inverted pencil cup, placed in the center area) for 10 min, then was returned to its home cage. The apparatus was cleaned and a social stimulus (an age- and sex-matched mouse) was placed inside the capsule. The test animal was put back into the apparatus to explore for 10 min. The time spent interacting with the social stimulus was measured.

Locomotion test. Animals were placed in a cage (L: 42 cm, W: 20 cm, H: 20 cm) devoid of any bedding materials for 5 min and the number of times crossing a midline was counted.

Rotarod test. To assess motor coordination and balance, an accelerating rotarod (San Diego Instruments, San Diego CA) was used. Mice were placed on a cylinder, which slowly accelerated from 4 to 40 r.p.m. over a 5-min test session. The task requires mice to walk forward in order to remain on top of the rotating cylinder rod.

Self-grooming. Mice were scored for spontaneous grooming behaviors when placed individually in a clean cage. The cage was lined with a thin layer of bedding (~1 cm) in order to reduce neophobia but prevent digging, a potentially competing behavior. Prior to the testing period, animals were allowed to habituate to the novel environment for 10 min. Each mouse was rated for 10 min on cumulative time spent grooming.

Open-field test. Animals were placed in a rectangular arena (60 cm×80 cm); the amount of time the animal spent in the center (25 cm×25 cm) was counted. Anxious animals spend less time in the center and more time in the corner of the field.

Western blotting of nuclear, synaptic and total proteins. Nuclear extracts from mouse brains were prepared according to the manufacturer's instructions (Life Technologies) with modifications. Briefly, ten PFC punches (diameter: 2 mm) from fresh mouse slices (300 μm) per animal were collected, and then homogenized with 500 μL homogenization buffer (20 mM Tris-HCl, pH 7.4, 10 mM NaCl, 3 mM $MgCl_2$, 0.5% NP-40, 1 mM PMSF, with cocktail protease inhibitor). The homogenate was incubated on ice for 15 min and followed by centrifugation at 3,000 *g*, 4 °C for 10 min. The nuclear pellet was resuspended in 50 μL nuclear extract buffer (100 mM Tris-HCl, pH 7.4, 100 mM NaCl, 1 mM EDTA, 1% Triton X-100, 0.1% SDS, 10% glycerol, 1 mM PMSF, with cocktail protease inhibitor) and incubated on ice for 30 min with periodic vortexing to resuspend the pellet. After centrifugation, the supernatant for nuclear fractions was collected, boiled in 2×SDS loading buffer for 5 min and then separated on 10% SDS-polyacrylamide gels. Western blotting experiments for nuclear proteins were performed with antibodies against acetylated H3K9 (1:1,000, Cell Signaling, 9649), H3 (1:500, Cell Signaling Technology, 4499), HDAC1 (1:500, Santa Cruz Biotech., sc-7872), HDAC2 (1:500, Santa Cruz Biotech., sc-7899) and β-catenin (1:1,000, Cell Signaling, 8480) as previously described[43,44].

Synaptic membrane and cytosolic fractions were prepared as described previously[12]. In brief, blocks of frontal cortex were cut out, weighed and homogenized in ice-cold lysis buffer (10 mL/g, 15 mM Tris, pH 7.6, 0.25 M sucrose, 1 mM PMSF, 2 mM EDTA, 1 mM EGTA, 10 mM Na_3VO_4, 25 mM NaF, 10 mM sodium pyrophosphate and protease inhibitor tablet). After centrifugation at 800 *g* for 5 min to remove nuclei and large debris, the remaining supernatant was subjected to 10,000 *g* centrifugation for 10 min. The crude synaptosome fraction (pellet) was suspended in lysis buffer containing 1% Triton X-100 and 300 mM NaCl, homogenized again and centrifuged at 16,000 *g* for 15 min. The Triton insoluble fraction, which mainly includes membrane-associated proteins from synaptosomes, was dissolved in 1% SDS. Samples were boiled in 2×SDS loading buffer for 5 min and separated on 7.5% SDS-PAGE. Anti-β-catenin (1:1,000, Cell Signaling, 8480) was used to detect β-catenin in the synaptic membrane fraction, and anti-non-phosphorylated β-catenin (1:1,000, Cell Signaling, 8814) was used to detect the active form of β-catenin in the cytosol.

Western blotting of total proteins[12,43] was performed using antibodies against NR1 (1:500, NeuroMab, 75-272), NR2A (1:500, Millipore, 07-632), NR2B (1:500, Millipore, 06-600), GluR1 (1:500, Millipore, AB1504), GluR2 (1:500, NeuroMab 75-002), Shank3 (1:500, NeuroMab, 75-344, clone N367/62), tubulin (Sigma, T9026), βPIX (1:500, Santa Cruz Biotechnology, sc393814), LIMK (1:1,000, BD Biosciences, 611748), cortactin (1:1,000, Cell Signaling, #3502), CTTNBP2 (1:1,000, Proteintech Group, 17893), Ank2 (1:500, NeuroMab clone N105/17) and SYNGAP (1:1,000, Cell Signaling, #9479).

Co-immunoprecipitation (Co-IP). Frontal cortical slices from WT mice were collected and homogenized in lysis buffer (in mM: 50 NaCl, 30 sodium pyrophosphate, 50 NaF, 10 Tris, 5 EDTA, 0.1 Na_3VO_4, 1 PMSF, with 1% Triton X-100 and protease inhibitor tablet). Lysates were centrifuged (12,000 *g*) at 4 °C for 15 min. Supernatant fraction was incubated with the antibody against β-catenin (8 μL, Cell Signaling, 2698) overnight at 4 °C (negative controls used the antibody against mouse IgG (Millipore, 12-371) or no antibody), followed by incubation with 50 μL of protein A/G plus agarose (Santa Cruz Biotech., sc-2003) for 1 h at 4 °C. Immunoprecipitates were washed three times with lysis buffer, then boiled in 2×SDS loading buffer for 5 min and separated on 7.5% SDS-polyacrylamide gels. Western blotting experiments were performed with anti-Shank3 (1:1,000, Abcam, ab101919) and anti-β-catenin (1:1,000, Cell Signaling, 2698).

Chromatin immunoprecipitation (ChIP). Briefly, ten PFC punches from brain slices per two animals were collected, cross-linked with 1% formaldehyde for 12 min and quenched by the addition of glycine at a final concentration of 0.125 M for 5 min before freezing at −80 °C. The chromatin was extracted by the 1% SDS lysis buffer, followed by shearing with a Fisher Scientific Sonic Dismembrator Model 300 at 28% power (ten 15-s pulses with a 30 s pause between pulses). This procedure resulted in DNA fragment sizes of 200–500 bp. After centrifugation, ~10% of the supernatant was saved to serve as input controls. To reduce nonspecific background, the supernatant was diluted in ChIP dilution buffer and precleared with 80 μL salmon sperm DNA/protein A agarose 50% slurry (Millipore, 16-157) for 30 min at 4 °C with agitation. The precleared supernatant was incubated with antibodies against β-catenin (Cell Signaling, 8480, 20 μL per reaction) or pan-acetylated H3 (Millipore, 06-599, 7 μg per reaction) overnight at 4 °C under constant rotation, followed by incubation with 60 μL of salmon sperm DNA/Protein A agarose 50% slurry for 1 h at 4 °C. Rabbit IgG was used as a nonspecific control for immunoprecipitation assays. After washing five times, the bound complex was eluted from the beads by incubating with 150 μL elution buffer twice at room temperature (23 °C). After reversing crosslinks in 65 °C for 4 h, proteins and RNA were removed using proteinase K (Invitrogen) and RNase

(Roche), respectively. Then immunoprecipitated DNA and input DNA were purified by phenol/chloroform extraction. Quantification of ChIP signals was calculated as percent input.

Primers from multiple sites relative to TSS (within 2000 bp) were designed and pretested in both input and ChIP samples. Only those with solid signals in both input and ChIP samples were chosen for the experiment. Purified DNA was subjected to qPCR reactions with primers against mouse *HDAC2* promoter (forward, −1,748 bp to −1,728 bp relative to TSS, 5′-GGGTTGCAGACCCCTTTAGT-3′; reverse, −1,566 bp to −1,546 bp relative to TSS, 5′-TCACAAGAGGACAAGCCGAC-3′); *GAPDH* promoter (forward, −441 bp to −422 bp relative to TSS, 5′-GCATTCAGGTCTCTGGGTCC-3′; reverse, −295 bp to −276 bp relative to TSS, 5′-GTGGGCTCCGAACTGATAGG-3′); *Grin2a* promoter (forward, −112 bp to −93 bp relative to TSS, 5′-CCCGCTCTGAGAGTCGAATG-3′; reverse, −233 bp to −214 bp relative to TSS, 5′-GGCAAAATAGCTCGGCTTGG-3′), *Grin2b* promoter (forward, −733 bp to −712 bp relative to TSS, 5′-AGATTTGAGGACTTTGGGGTTC-3′; reverse, −833 bp to −813 bp relative to TSS, 5′-GCTGGGTTAGTCAGTGCTGTA-3′), *Arhgef7* promoter (forward, −950 bp to −932 bp relative to TSS, 5′-AAACTGTCGAGGAGTGCCAG-3′; reverse, −749 bp to −730 bp relative to TSS, 5′-TCAAGAGCACATCGCAACCT-3′) and *Limk1* promoter (forward, −644 bp to −625 bp relative to TSS, 5′-TTCCGCTGTTCACAGACTCC-3′; reverse, −447 bp to −428 bp relative to TSS, 5′-ATAACCACGCCCATCAAGCA-3′).

Quantitative real-time PCR. To compare the mRNA levels, quantitative RT-PCR was used. Total RNA was isolated from mouse PFC punches using Trizol reagent (Invitrogen) and treated with DNase I (Invitrogen) to remove genomic DNA. Then SuperScript III first-strand synthesis system for RT-PCR (Invitrogen) was used to obtain cDNA from the tissue mRNA, followed by the treatment with RNase H (2 U/ l) for 20 min at 37 °C. Quantitative RT-PCR was carried out using the iCycler iQ Real-Time PCR Detection System and iQ Supermix (Bio-Rad) according to the manufacturer's instructions. In brief, *Gapdh* was used as the housekeeping gene for quantitation of the expression of target genes in samples from WT and Shank3$^{+/\Delta C}$ mice treated with romidepsin or saline control. Fold changes in the target genes were determined by: Fold change $= 2^{-\Delta(\Delta C_T)}$, where $\Delta C_T = C_{T(\text{target})} - C_{T(\text{Gapdh})}$, and $\Delta(\Delta C_T) = \Delta C_{T(\text{treated group})} - \Delta C_{T(\text{WT + saline})}$. C_T (threshold cycle) is defined as the fractional cycle number at which the fluorescence reaches 10 × the s.d. of the baseline. A total reaction mixture of 25 µL was amplified in a 96-well thin-wall PCR plate (Bio-Rad) using the following PCR cycling parameters: 95 °C for 5 min followed by 40 cycles of 95 °C for 30 s, 55 °C for 30 s and 72 °C for 60 s. Primers for all target genes are listed in Supplementary Table 3.

Immunohistochemistry. Mice were anesthetized and transcardially perfused with PBS, followed by 4% paraformaldehyde (PFA) before brain removal. Brains were postfixed in 4% PFA for 2 d and cut into 100-µm slices. Slices were cut coronally and permeabilized using 0.5% Triton in PBS for 1 h, washed and blocked for 1 h in PBS containing 3% BSA and 0.3% Triton. After washing, slices were incubated with the primary antibody against CaMKII (1:500, Santa Cruz Biotechnology, sc-9035), NeuN (1:1,000, Millipore, MAB377) or PSD-95 (Neuromab, 75-028, 1:1,000) for 48 h at 4 °C. After washing three times (0.5 h, 1 h and 1 h with gentle shaking) in PBS, slices were incubated with one or two secondary antibodies (Alexa Fluor 488, Invitrogen, A21202, 1:1,000; or Alexa Fluor 594, Invitrogen A11032) for 1 h at room temperature, followed by three washes with PBS. For F-actin staining, slices were then incubated with DAPI antibody (1:10,000) for 10 min at room temperature, followed by three washes with PBS. Slices were mounted on slides with Vectashield mounting media (Vector Laboratories). Images were acquired using a 40 × objective on a Zeiss LSM 510 confocal microscope. All specimens were imaged under identical conditions and analyzed with identical parameters using Image J software. *Z*-axis stacked confocal images (10) of 9 PFC areas (225 µm × 225 µm) from 3–4 slices per animal were quantified.

Electrophysiological recordings. Whole-cell voltage-clamp recording was used to measure synaptic currents in layer V pyramidal neurons of PFC slices, as previously described[12,43]. Mouse brain slices (300 µm) were positioned in a perfusion chamber attached to the fixed stage of an upright microscope (Olympus) and submerged in continuously flowing oxygenated ACSF (in mM: 130 NaCl, 26 $NaHCO_3$, 1 $CaCl_2$, 5 $MgCl_2$, 3 KCl, 1.25 NaH_2PO_4, 10 glucose, pH 7.4, 300 mOsm). Bicuculline (20 µM) and CNQX (20 µM) were added in NMDAR-EPSC recordings. Bicuculline and D-APV (50 µM) were added in AMPAR-EPSC recordings. Patch electrodes contained the following internal solution (in mM): 130 cesium-methanesulfonate, 10 CsCl, 4 NaCl, 10 HEPES, 1 $MgCl_2$, 5 EGTA, 2 QX-314, 12 phosphocreatine, 5 MgATP, 0.2 Na_3GTP, 0.1 leupeptin, pH 7.2–7.3, 265–270 mOsm. Layer V mPFC pyramidal neurons were visualized with a 40 × water-immersion lens and recorded with the Multiclamp 700 A amplifier (Molecular Devices, Sunnyvale, CA). Evoked synaptic currents were generated with a pulse from a stimulation isolation unit controlled by an S48 pulse generator (Grass Technologies, West Warwick, RI). A bipolar stimulating electrode (FHC, Bowdoinham, ME) was placed ~100 µm from the neuron under recording. For NMDAR-EPSC, the cell (clamped at −70 mV) was depolarized to + 40 mV for 3 s before stimulation to fully relieve the voltage-dependent Mg^{2+} block. Membrane potential was maintained at −70 mV for AMPAR-EPSC recordings. For input–output responses, synaptic currents were elicited by a series of pulses with varying stimulation intensities (50–90 µA) delivered at 0.05 Hz. To obtain the NMDAR- to AMPAR-EPSC ratio, AMPAR-EPSC were first recorded at −70 mV in ACSF solution (containing bicuculline). Then the mixture of AMPAR-EPSC and NMDAR-EPSC was recorded at + 40 mV with the same stimulation pulse (0.4 ms, 70 µA). The peak of NMDAR-EPSC was calculated at 40 ms from the onset of the EPSC mixture.

Virus generation and delivery. The shRNA oligonucleotide targeting mouse *HDAC2* sequence (CCCAATGAGTTGCCATATAAT, Open Biosystem) was inserted in the lentiviral vector pLKO.3 G (Addgene), which contains an eGFP marker. For the production of lentiviral particles, a mixture containing the pLKO.3 G shRNA plasmid (against *HDAC2*), psPAX2 packaging plasmid and pMD2.G envelope plasmid (Addgene) was transfected to HEK-293FT cells using Lipofectamine 2000. The transfection reagent was removed 12–15 h later, and cells were incubated in fresh DMEM (containing 10% FBS + penicillin/streptomycin) for 24 h. The media harvested from the cells, which contained lentiviral particles, was concentrated by centrifugation (2,000 *g*, 20 min) with Amicon Ultra Centrifugal Filter (Ultracel-100K, Millipore). The concentrated virus was stored at −80 °C. Another shRNA lentivirus targeting different sequences of the mouse *HDAC2* gene (CATGAGAGATGGTATAGAT, GCTTGGTTGTTTCAATCTA, ACATGCACCTGGTGTTCAA) was obtained from Santa Cruz Biotech (sc-29346-V). The GFP-tagged β-catenin adenovirus was obtained from Vector Biolabs (1182). The shRNA lentivirus targeting mouse *beta-catenin* gene (GCCTTCAGATCTTAGCTTA, CAGCTGGAATTCTCTCTAA, CTGCAGAACTCCAGAAAGA, GTCGAGGAGTAACAATACA) was obtained from Santa Cruz Biotech (sc-29210-V). In vivo delivery of the viral suspension (1 µL each side) was achieved by stereotaxic injection bilaterally into medial PFC (2.0 mm anterior to bregma; 0.25 mm lateral) with a Hamilton syringe (needle gauge 31, extended to a depth of 2.0 mm below the tissue surface) as previously described[12,44].

RNA sequencing and bioinformatic analysis. PFC samples were obtained from three WT mice, three saline-treated Shank3$^{+/\Delta C}$ mice and two romidepsin-treated Shank3$^{+/\Delta C}$ mice. We generated strand-specific RNA libraries from 1 µg purified RNA using TruSeq Stranded Total RNA Plus Ribo-zero kits (Illumina). Sequencing was performed at the Genomics and Bioinformatics Core of the State University of New York at Buffalo. Single-end reads per sample were obtained using the HiSeq 2500 platform from Illumina. Reads were first trimmed using Cutadapt[45] to remove the 3′ end adapters and trailing sequences, followed by aligning to mouse RefSeq mRNAs using TopHat2[46]. Transcript counts were estimated using HTSeq[47]. Differences in gene expression levels between samples were assessed with edgeR[48] and calculated as log2 fold-changes. Functional enrichment analyses of differentially expressed genes were undertaken using gene sets derived from the Biological Process Ontology from GSEA (http://software.broadinstitute.org/gsea/msigdb/index.jsp).

Statistics. Data analyses were performed with Clampfit (Molecular Devices, Sunnyvale, CA), KaleidaGraph (Synergy Software, Reading, PA) and GraphPad Prism 6 (GraphPad Software, Inc., La Jolla, CA). For statistical significance, experiments with two groups were analyzed using two-tailed Student's *t* tests. Experiments with more than two groups were subjected to one-way ANOVA, two-way ANOVA or two-way repeated measurea ANOVA (rmANOVA), followed by post hoc Bonferroni tests for multiple comparisons. Measurements were taken from distinct samples. No sample was excluded from the analysis. Sample sizes were based on power analyses and were similar to those reported in previous works[12,43,44]. We tested the normality and variance of data distribution between groups being statistically compared. Data in box plots are presented as: center line, median; box limits, upper and lower quartiles; whiskers, minimal and maximum values. Data in all other formats are presented as mean ± s.e.m. *F* values, degrees of freedom and *P* values for all ANOVAs (unless otherwise stated, they represent statistics of main interaction effects and post hoc comparisons), as well as *t*-values and degrees of freedom for *t* tests, are included in figure legends.

Accession codes. Accession codes have been deposited at GEO: GSE109328.

Life Science Reporting Summary. Further information on experimental design and reagents is available in the Life Sciences Reporting Summary.

Data availability. The data that support the findings of this study are available from the corresponding author upon reasonable request.

References

43. Yuen, E. Y. et al. Repeated stress causes cognitive impairment by suppressing glutamate receptor expression and function in prefrontal cortex. *Neuron* **73**, 962–977 (2012).
44. Wei, J. et al. Histone modification of *Nedd4* ubiquitin ligase controls the loss of AMPA receptors and cognitive impairment induced by repeated stress. *J. Neurosci.* **36**, 2119–2130 (2016).

45. Marcel, M. Cutadapt removes adapter sequences from high-throughput sequencing reads. *EMBnet.journal* **17**, 10–12 (2011).
46. Kim, D. et al. TopHat2: accurate alignment of transcriptomes in the presence of insertions, deletions and gene fusions. *Genome Biol.* **14**, R36 (2013).
47. Anders, S., Pyl, P. T. & Huber, W. HTSeq–a Python framework to work with high-throughput sequencing data. *Bioinformatics* **31**, 166–169 (2015).
48. Robinson, M. D., McCarthy, D. J. & Smyth, G. K. edgeR: a Bioconductor package for differential expression analysis of digital gene expression data. *Bioinformatics* **26**, 139–140 (2010).

nature research

Corresponding author(s): Zhen Yan

☐ Initial submission ☐ Revised version ☒ Final submission

Life Sciences Reporting Summary

Nature Research wishes to improve the reproducibility of the work that we publish. This form is intended for publication with all accepted life science papers and provides structure for consistency and transparency in reporting. Every life science submission will use this form; some list items might not apply to an individual manuscript, but all fields must be completed for clarity.

For further information on the points included in this form, see Reporting Life Sciences Research. For further information on Nature Research policies, including our data availability policy, see Authors & Referees and the Editorial Policy Checklist.

Experimental design

1. Sample size

Describe how sample size was determined.

Sample sizes were based on power analyses and previous experiments conducted by us (Yuen EY et al., Neuron 73:962-77, 2012; Duffney LJ et al., Cell Reports 11:1400-1413, 2015; Wei J et al., J. Neuroscience 36:2119-30, 2016) and many other labs in the field.

2. Data exclusions

Describe any data exclusions.

No data was excluded in analysis.

3. Replication

Describe whether the experimental findings were reliably reproduced.

We listed the number of times we repeated the experiments in figure legends. The behavioral phenotypes reported here (by K. Ma) were independently replicated by 3 other lab members (Drs. M. Rapanelli, Z-J Wang, and L. Duffney).

4. Randomization

Describe how samples/organisms/participants were allocated into experimental groups.

Mice of different genotypes were randomly assigned to drug/saline groups.

5. Blinding

Describe whether the investigators were blinded to group allocation during data collection and/or analysis.

The investigator was blinded to the group allocation (with no prior knowledge about the genotypes and treatments) during the experiments.

Note: all studies involving animals and/or human research participants must disclose whether blinding and randomization were used.

6. Statistical parameters

For all figures and tables that use statistical methods, confirm that the following items are present in relevant figure legends (or in the Methods section if additional space is needed).

n/a	Confirmed
☐	☒ The exact sample size (*n*) for each experimental group/condition, given as a discrete number and unit of measurement (animals, litters, cultures, etc.)
☐	☒ A description of how samples were collected, noting whether measurements were taken from distinct samples or whether the same sample was measured repeatedly
☐	☒ A statement indicating how many times each experiment was replicated
☐	☒ The statistical test(s) used and whether they are one- or two-sided (note: only common tests should be described solely by name; more complex techniques should be described in the Methods section)
☐	☒ A description of any assumptions or corrections, such as an adjustment for multiple comparisons
☐	☒ The test results (e.g. *P* values) given as exact values whenever possible and with confidence intervals noted
☐	☒ A clear description of statistics including central tendency (e.g. median, mean) and variation (e.g. standard deviation, interquartile range)
☐	☒ Clearly defined error bars

See the web collection on statistics for biologists for further resources and guidance.

Software

Policy information about availability of computer code

7. Software

Describe the software used to analyze the data in this study.	Data analyses were performed with Clampfit, Kaleidagraph and GraphPad Prism 6. Experiments with two groups were analyzed statistically using two-tailed Student's t-tests. Experiments with more than two groups were subjected to one-way ANOVA, two-way ANOVA, or two-way repeated measure ANOVA (rmANOVA), followed by post hoc Bonferroni tests. We described this in the Method section of the manuscript.

For manuscripts utilizing custom algorithms or software that are central to the paper but not yet described in the published literature, software must be made available to editors and reviewers upon request. We strongly encourage code deposition in a community repository (e.g. GitHub). *Nature Methods* guidance for providing algorithms and software for publication provides further information on this topic.

Materials and reagents

Policy information about availability of materials

8. Materials availability

Indicate whether there are restrictions on availability of unique materials or if these materials are only available for distribution by a for-profit company.	All materials are available upon execution of Material Transfer Agreement and any agreements related to commercial development if applicable.

9. Antibodies

Describe the antibodies used and how they were validated for use in the system under study (i.e. assay and species).	Information on antibody is included in the Method section. The antibodies have been validated by vendors and by our own experiments. Western blotting: acetylated H3K9 (1:1000, Cell Signaling, 9649), H3 (1:500, Cell Signaling Technology, 4499), HDAC1 (1:500, Santa Cruz Biotech., sc-7872), HDAC2 (1:500, Santa Cruz Biotech., sc-7899), b-catenin (1:1000, Cell Signaling, 8480), non-phosphorylated b-catenin (1:1000, Cell Signaling, 8814), NR1 (1:500, NeuroMab, 75-272), NR2A (1:500, Millipore, 07-632), NR2B (1:500, Millipore, 06-600), GluR1 (1:500, Millipore, AB1504), GluR2 (1:500, NeuroMab 75-002), Shank3 (1:500, NeuroMab, 75-344, clone N367/62), tubulin (Sigma, T9026), bPIX (1:500, Santa Cruz Biotechnology, sc393814), LIMK (1:1000, BD Biosciences, 611748), Cortactin (1:1000, Cell Signaling, 3502), CTTNBP2 (1:1000, Proteintech Group, 17893), Ank2 (1:500, NeuroMab clone N105/17), and SYNGAP (1:1000, Cell Signaling, 9479). IP-WB: b-catenin (8 µl, Cell Signaling, 2698), Shank3 (1:1000, Abcam, ab101919). ChIP: b-catenin (Cell Signaling, 8480, 20 µl per reaction), pan-acetylated H3 (Millipore, 06-599, 7 µg per reaction). Immunohistochemistry: CaMKII (1:500, Santa Cruz Biotechnology, sc-9035), NeuN (1:1000, Millipore, MAB377), PSD-95 (Neuromab, 75-028, 1:1000)

10. Eukaryotic cell lines

a. State the source of each eukaryotic cell line used.	No cell lines were used.
b. Describe the method of cell line authentication used.	n/a
c. Report whether the cell lines were tested for mycoplasma contamination.	n/a
d. If any of the cell lines used are listed in the database of commonly misidentified cell lines maintained by ICLAC, provide a scientific rationale for their use.	n/a

Animals and human research participants

Policy information about studies involving animals; when reporting animal research, follow the ARRIVE guidelines

11. Description of research animals

Provide details on animals and/or animal-derived materials used in the study.

Heterozygous Shank3+/ΔC mice expressing C-terminal (exon 21) deleted Shank3 (Jackson Labs, Bar Harbor, ME) (5-8 weeks old, male) and age-matched wild-type littermates (male) were used in this study. Female Shank3+/ΔC mice lack the autism-like social deficits, so they were not used. In some experiments, homozygous Shank3(e4-9) mice (provided by Dr. YH Jiang in Duke University) (5-6 weeks old, male and female) were used. All experiments were performed with the approval of the Institutional Animal Care and Use Committee (IACUC) of the State University of New York at Buffalo.

Policy information about studies involving human research participants

12. Description of human research participants

Describe the covariate-relevant population characteristics of the human research participants.

There are no human research participants.